UNIVERSITY OF ALBERTA

FACULTY OF GRADUATE STUDIES AND RESEARCH

LIFETIME MEASUREMENTS FOR MnII AND CrII LEVELS

USING THE BEAM-LASER METHOD

BY

© QING JI

A THESIS

SUBMITTED TO THE FACULTY OF GRADUATE STUDIES AND
RESEARCH IN PARTIAL FULFILLMENT OF THE REQUIREMENT FOR THE
DEGREE OF MASTER OF SCIENCE

IN

ASTROPHYSICS

DEPARTMENT OF PHYSICS

EDMONTON, ALBERTA

SPRING 1993

Canada

UNIVERSITY OF ALBERTA

RELEASE FORM

NAME OF AUTHOR: QING JI

TITLE OF THESIS: LIFETIME MEASUREMENTS FOR MnII AND CrII

LEVELS USING THE BEAM-LASER METHOD

DEGREE: MASTER OF SCIENCE

YEAR THIS DEGREE GRANTED: 1993

PERMISION IS HERBY GRANTED TO THE UNIVERSITY OF ALBERTA LIBRARY TO REPRODUCE SINGLE COPIES OF THIS THESIS AND TO LEND OR SELL SUCH COPIES FOR PRIVATE, SCHOLARLY OR SCIENTIFIC REASEARCH ONLY.

THE AUTHOR RESERVES OTHER PUBLICATION RIGHTS, AND NEITHER THE THESIS NOR EXTENSIVE EXTRACTS FROM IT MAY BE PRINTED OR OTHERWISE REPRODUCED WITHOUT THE AUTHOR'S WRITTEN PERMISSION.

(Student's signature)

Physics Department
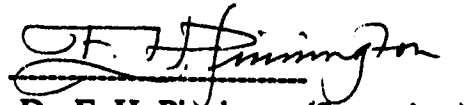
University of Alberta
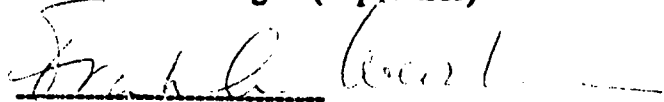
Edmonton, Alberta T6G 2J1

Date: Jan. 20, 1993

UNIVERSITY OF ALBERTA

FACULTY OF GRADUATE STUDIES AND RESEARCH

THE UNDERSIGNED CERTIFY THEY HAVE READ, AND RECOMMEND TO
THE FACULTY OF GRADUATE STUDIES AND RESEARCH FOR
ACCEPTANCE, A THESIS ENTITLED LIFETIME MEASUREMENTS FOR MNII
AND CRII LEVELS USING THE BEAM-LASER METHOD
SUBMITTED BY QING JI
IN PARTIAL FULFILLMENT OF THE REQUIREMENTS FOR THE DEGREE
OF MASTER OF SCIENCE IN PHYSICS(ASTROPHYSICS)

Dr. E. H. Pinnington(Supervisor)

Dr. F. Weichman

Dr. J. A. Kernahan

Dr. G. Horlick

Date: Jan. 20, 1993

Abstract

The lifetimes of the z^5P and z^7P levels of MnII and the z^6F, z^6D, z^6P, z^4P and z^4D levels of CrII have been measured by using the beam-laser technique. The results are systematically longer than those derived from Kurucz's calculated gf-values for these levels. Therefore corrections to Kurucz's gf-values by these experimental results have been suggested. Based on these corrections to the gf-values, the elemental abundances of manganese and chromium in the solar atmosphere can be recalculated. The beam-laser technique, as the most reliable and accurate method for lifetime measurements, is introduced in detail. Laser excitation of a fast ion beam is an important process in the beam-laser method. This process can not be described by the rate-equation theory due to the laser radiation used in these experiments being very intense. The condition for saturated excitation of the beam can be derived from a two level system model by a semi-classical theory.

ACKNOWLEDGEMENTS

TABLE OF CONTENTS

LIST OF FIGURES

LIST OF TABLES

CHAPTER ONE

INTRODUCTION

1.1 Introduction

The absolute oscillator strengths of atomic and ionic spectral lines are of great interest in the calculation of the properties of gas discharges, plasmas or stellar atmospheres. In astrophysics, determination of the abundance of different elements in the solar atmosphere requires accurate knowledge of oscillator strengths for both neutral and ionized atoms. The absolute oscillator strengths can be obtained by both theoretical calculations and experimental measurements. Since it is usually difficult to know the uncertainties in theoretical calculations, experimental results should be used to test them. Obviously, for a significant test of the calculations, it is essential that the lifetime measurements be sufficiently accurate.

For the experimental measurement of oscillator strengths, two methods are usually used. One is to measure absolute oscillator strengths directly from the emission of plasmas close to or in thermodynamical equilibrium. The uncertainty in such a method is typically at least 25%[25]. The second,more reliable, approach is a combination of precise lifetime measurements with experimental or theoretical branching

ratios. The uncertainty of branching ratios from careful experiments is typically 2-5%[21][23]. Therefore, the accuracy of oscillator strengths mainly depends on the lifetime measurements. So we can say that precise lifetime measurements play an important role in the theoretical and experimental determination of oscillator strengths.

Many different techniques have been developed for the purpose of measuring atomic lifetimes. A large number of atomic states have been measured by the beam-foil method[2], which has the advantage of good time resolution. The ion beam from an accelerator bombards a very thin solid foil, usually a carbon foil, and is excited to different stages of ionization. The excited species will decay by fluorescence as they move along the beam. The atomic lifetime can be obtained by measuring the intensity of fluorescence as a function of distance downstream from the foil. Because the beam-foil excitation process is not selective, cascading into the level of interest from higher levels leads to the observation of multi-exponential decay curves in which the number of components is generally not known. This makes it very difficult to derive an accurate lifetime from the measured decay curve.

The laser excitation process is selective, and so the beam-laser technique was developed to overcome the difficulty of

cascading in the beam-foil method. The accuracy for the beam-laser method is typically 1-3%[12], although in favourable circumstances, accuracies as high as 0.15% have been reported[9].

The research program of the atomic physics group at the University of Alberta has been involoved in precise lifetime measurements by the beam-laser method in recent years. Since 1985, lifetimes of some levels of CaII, MgII, NaII and TiII have been measured[1][12]. The NaII and TiII lifetimes were measured by using the 308 nm radiation from the XeCl excimer laser itself. The CaII measurements used radiation close to 395nm produced by a tunable dye laser. The MgII levels were populated using radiation from a KDP frequency-doubling crystal to achieve the required 280nm radiation. With improvement in experimental facilities, especially the acquisition of a B3O crystal, research has turned towards shorter wavelengths for transitions in the singly-ionized iron group elements. Atomic levels of FeII, MnII and CrII have been measured in the last few years. These results show the advantage of the beam-laser method. The accuracy obtained, even for the weakest transitions studied, is about 3%. Some of the results have been used for the calculation of solar abundances and the testing of complex quantum mechanical calculations[24].

This work is largely a team effort involving several members of the atomic physics group. I joined this group in 1991 as a graduate student in the M.Sc program. Since then I have been engaged in the lifetime measurements of the singly-ionized iron group elements. I have taken part in some of the experiments for FeII and most of the work for MnII. As the main part of my thesis work, I have focused on the CrII experiments, making significant contributions to all stages: the literature survey, preparations for the experiment, acquisition of data and analysis of the results.

In this thesis, I will give a brief outline of the experimental procedures in Chapter 2. Some of the problems encountered in these experiments are also discussed. Chapter 3 presents experimental results for MnII and CrII. The astrophysical implications of these results are also introduced. Chapter 4 describes the laser excitation process for the fast beam by a quantum mechanical calculation. Some of the problems associated with this process are discussed. Finally, in Chapter 5, I give a summary of this project. Possible future directions for these experiments are also discussed.

CHAPTER TWO

EXPERIMENTAL METHOD

This Chapter gives a brief description of the beam-laser method. The techniques used to obtain a decay curve, and to analyze the decay curve and derive an accurate lifetime with this method, are described in more detail.

2.1 Experimental Arrangement

The beam-laser method is based on the idea of converting a time-dependent decay process into a spatial variation of fluorescence intensity and on the fact that atoms can be selectively excited to a single level of interest. After the ions in the beam are excited to a specific level by a laser, they will decay by fluorescence as they move along the beam. The intensity of fluorescence decreases exponentially with the distance downstream. A measurement of the intensity of fluorescence as a function of distance gives the lifetime of the excited level. Because of their high velocity, the excited ions can move several millimetres downstream as they decay. This not only makes it possible to separate the fluorescence signal from laser light scattered at the interaction region, but also gives good time resolution.

A schematic illustration of the experimental arrangement is

shown in Fig(2.1-1). The experimental set-up includes three major parts: the accelerator and ion beam system, the laser system and the fluorescence detection and data collecting system.
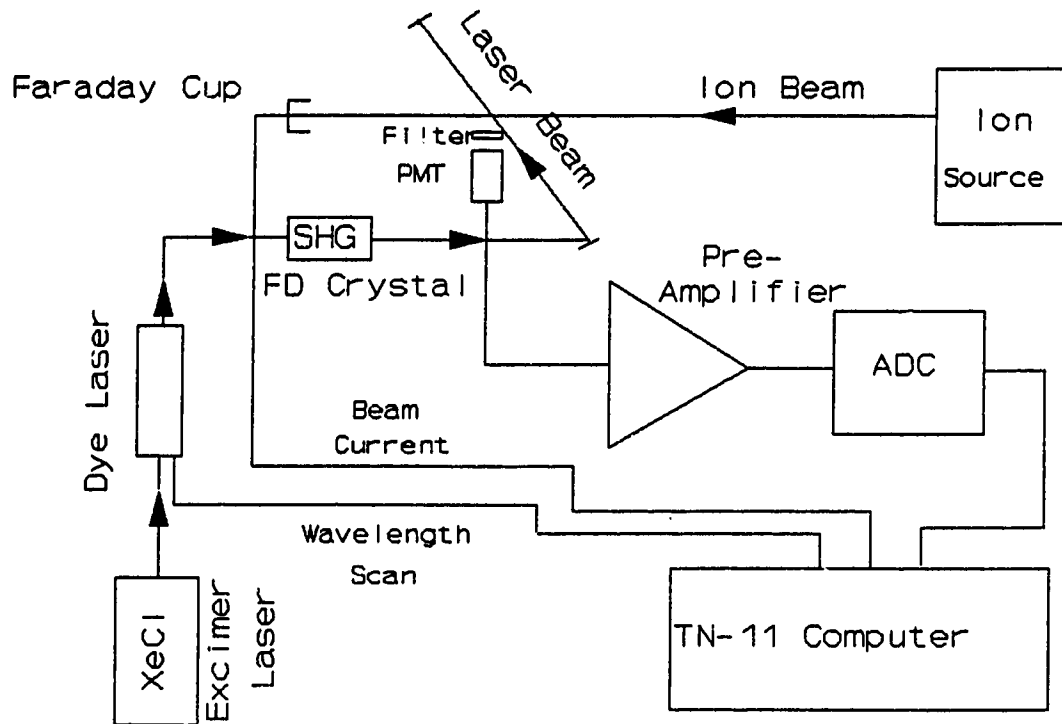
Fig.2.1-1 The beam laser experimental arrangement

The accelerator and ion beam system is composed of a 350 keV linear accelerator equipped with a Danfysik 911a hollow cathode ion source, a beam line equipped with a beam-profile monitor, a magnet for mass analysis and a target chamber. The whole system is evacuated by two pumping stations to about 5× 10^{-7} torr. The beam current is measured by a shielded Faraday

6

cup inside the target chamber. The maximum beam current of this system is typically 10 μA. The beam within the target chamber is defined by the 8 mm diameter aperture of the Faraday cup and a 5 mm diameter aperture at the entrance to the chamber. In an actual experiment, an accelerating voltage of typically around 290 kV is used. At that acceleration voltage, the beam velocity is about 1mm/ns. It is very important to maintain an adequate and stable beam current. Therefore control of the oven temperature and the pressure of the carrier gas is important for successful operation of the ion source. The filament in the ion source is easily broken and has to be replaced frequently, usually after about 5 hours of operation.

In order to be able to excite as wide a range of energy levels as possible, it is necessary to use a laser system which is tunable over a wide range of wavelengths. The laser system used in these experiments is a Lumonics EPD 330 dye laser pumped by a pulsed TE 860-3 XeCl excimer laser. The output wavelength of this laser is tunable by rotating a diffraction grating in the resonator. A combination of dyes can cover the wavelength range from 330 nm to 600 nm. Because most of the spectral lines for singly-ionized atoms of iron group are in the UV region, a BBO or KDP frequency-doubling crystal must be used to give tunable radiation from 220 nm to 330 nm. The excimer laser used to pump the dye is pulsed.

Under typical operating conditions, the average output power of the dye laser is 30 mW for a repetition rate of 75 Hz and about 5 ns laser pulse width. This corresponds to a peak power of 75 KW. In the earlier experiments of this project, a repetition rate of 250 Hz was used. Unfortunately, at the present time the maximum possible repetition rate is 80 Hz after major repairs to the gas circulator inside the excimer laser.

The fluorescence radiation from the laser-excited ion beam is collected by the optical detection system. For measuring decay curves this system is designed to move alternately parallel and anti-parallel to the beam direction. Details of this system are described in a previous thesis[10]. In order to reduce the background noise, an interference filter is often used in the optics of this system. The fluorescence is detected by a photomultiplier and the output of the photomultiplier is collected by charge-integration electronics, instead of the more usual single photon-counting electronics, because the single photon-counting technique is subject to the well-known problem of "pile up", i.e. it can not count more than one signal pulse for each laser pulse, irrespective of how many photons were collected to give that pulse. The total integrated charge was shaped and then sent to a gated analog-to-digital converter(ADC). This digitized signal was summed in a TN-11 data acquisition system.

2.2 Resonance fluorescence

The energy level of interest can be populated by laser radiation from the ground state, or a low-lying metastable state, by setting the laser frequency appropriate to the resonant frequency of the transition. When this level has been populated, it will decay by fluorescence. This is called resonant fluorescence. The lifetime of this level can be obtained from recording the intensity of resonance fluorescence as a function of the distance downstream from the excitation region, giving a fluorescence decay curve. So, before recording the decay curve, a very important step in this experiment is to achieve resonant excitation. This can be achieved by setting the laser at the wavelength appropriate to the transition of interest. This requires a fine scanning of the laser wavelength and an absolute wavelength calibration. The laser wavelength scanning is performed by rotating a diffraction grating inside the dye laser cavity through a stepping motor, which is controlled by the TN-11 computer. The step size for the scanning usually corresponds to 0.0005 to 0.001 nm. The absolute laser wavelength can be measured by a spectrometer, which is calibrated by a Neon or Krypton discharge lamp. The laser wavelength after the frequency doubling crystal is usually in the UV region (typically 220 nm to 300 nm) and the calibration spectral lines of the Neon or Krypton lamp are usually in the visible region (typically 450

nm to 760 nm). Therefore the second or third diffraction order of laser radiation is usually used for wavelength calibration. The wavelength accuracy obtained by this method is about 0.01 nm. The wavelength calibration is usually performed many times during the experiment because of the non-linearity of the scanning mechanism. It is certainly repeated each time a new laser resonant wavelength is chosen.

Because of the high velocity of the ion beam and a 45 degree intersection angle between ion beam and laser beam, there is a Doppler wavelength shift (usually 5 to 7 Å) between the observed laser wavelength at resonance and the atomic transition wavelength itself. This effect can be used for beam velocity calibration.

2.3 Velocity Calibration

The beam velocity is an important parameter, which must be measured in the beam-laser technique as accurately as possible. The most general way of measuring the beam velocity is to measure the Doppler shift between the wavelength of the laser radiation and the resonant atomic transition. In this experiment, the laser beam is arranged to intersect the ion beam at an angle of 45 degrees. By reflecting the laser back on itself, the ion beam can be excited by the laser on each passage. As shown in Fig(2.3-1), for the excitation from the

first passage the wavelength difference between the atomic transition and the laser radiation for a beam velocity v, is:

$$\Delta\lambda = -\lambda\frac{v}{c}cos45° \qquad (2.3-1)$$

where v is the beam velocity, and for the excitation from the reflected laser beam, the wavelength difference is:

$$\Delta\lambda = \lambda\frac{v}{c}cos45° \qquad (2.3-2)$$

Faraday Cup   Ion Beam

1 - Passage 1
2 - Passage 2
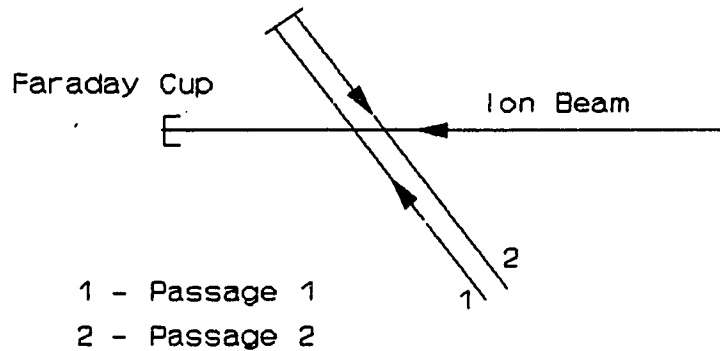
Fig.2.3-1 45 degree excitation of the beam

If $\Delta\lambda$ can be measured, the beam velocity v can be easily obtained:

$$v = \frac{c}{cos45°}\frac{\Delta\lambda}{\lambda} \qquad (2.3-3)$$

11

In practice it is difficult to measure the absolute resonant wavelength accurately because of the scarcity of
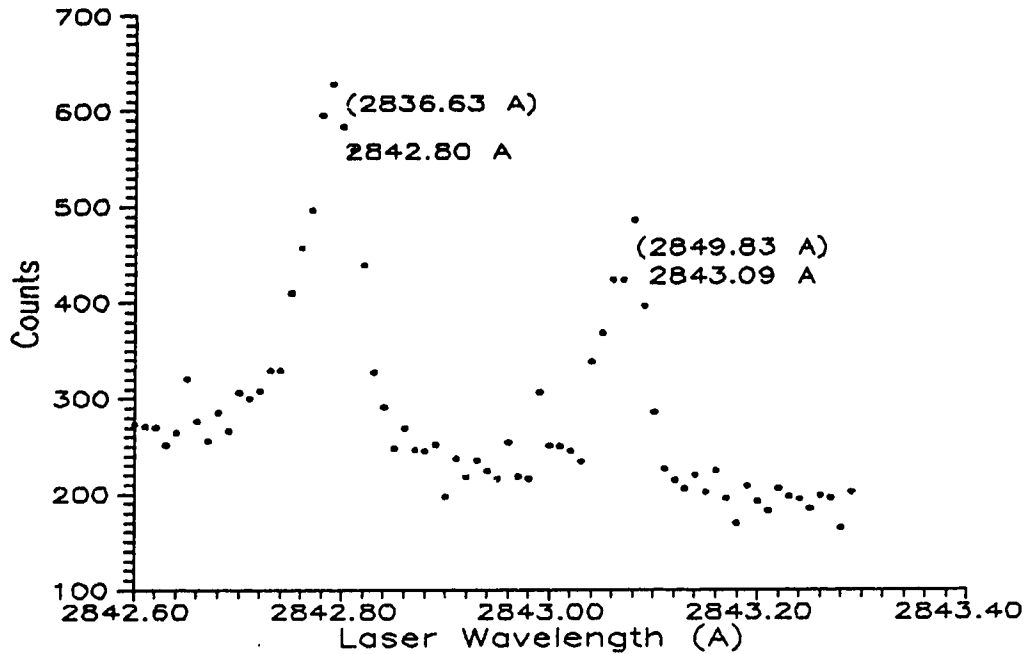
Fig.2.3-2 Two resonant lines for velocity calibration
in CrII expperiment

calibration lines and the non-linearity of the laser wavelength scanning mechanism. In order to overcome this difficulty, two atomic resonances are chosen in the velocity measurement. As shown in Fig(2.3-2), in which the figures in brackets are the unshifted wavelengths of the two atomic transitions, the resonance with longer wavelength is excited by the laser radiation from the first passage and the one with shorter wavelength is excited by the second passage. After Doppler shifts these two resonances are very close together.

12

The wavelength difference between the two laser resonances $\Delta\lambda_L$ is very small (of order 1-2 Å) and can be easily measured. The wavelength difference between the two atomic transitions $\Delta\lambda_0$ can be found from reference tables. Therefore the average wavelength difference between the laser resonance and atomic transition is:

$$\overline{\Delta\lambda} = \frac{\Delta\lambda_o - \Delta\lambda_L}{2} \qquad (2.3-4)$$

Substituting (2.3-4) into (2.3-3) gives the beam velocity. The important thing is that the two resonances should be chosen so that the wavelength difference between their atomic resonances is about twice the Doppler shift. The precision of this method is better than 1%.

2.4 Decay Curve Recording

A decay curve is obtained by measuring the intensity of fluorescence downstream along the ion beam. In order to minimize errors from slow variation in the laser power or ion beam current, the measurement is made by moving the detection system alternately parallel and anti-parallel to the beam direction. The first half of the decay curve contains a total of 29 data points which are recorded by moving the detection system parallel to the beam direction and the second half of

13

the decay curve contains 29 data points which are recorded from anti-parallel movement. One round trip movement is called
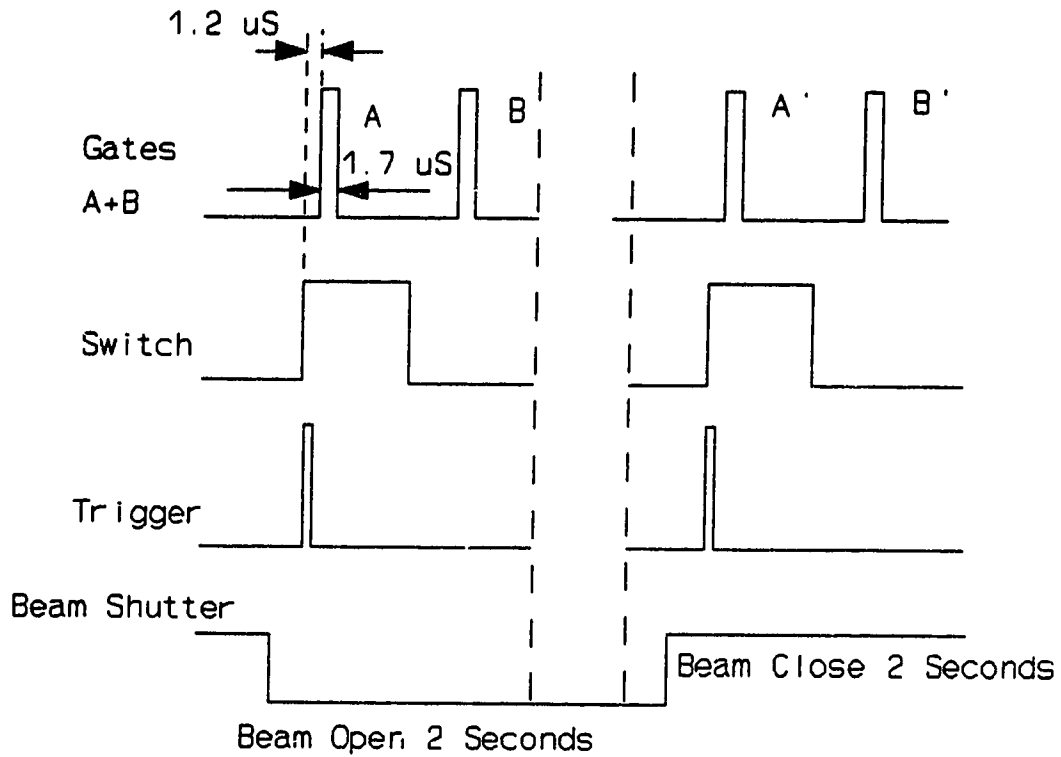
Fig.2.4-1 Timing sequence

a sweep. Several successive sweeps are summed to give the final decay curve. The step size between two adjacent data points is chosen according to the lifetime being measured.

The main source of noise comes from scattered light, which originates from two major sources. The first source of

scattered light is produced by the laser beam as it goes through the windows and the residual gas in the target chamber. The second is excitation of the ion beam by the residual gas in the target chamber, which gives rise to radiation over a wide range of wavelength. Although several measures are taken to minimize the scattered light, such as keeping a relatively low pressure in the target chamber and using a filter in front of the photomultiplier, the influence of scattered light still needs to be taken into account. The total scattered light signal must be subtracted from the total signal. So, for each data point, the experiment is designed to measure the total signal A, laser background B, beam-background A' and dark current B' in a time-sequence which is generated from the Tracor Northern TN-11 computer. As shown in Fig(2.4-1), in this designed time sequence, gating pulses are used to control the recording of the signal and background. When the beam is on (beam shutter is open), a triggering pulse is used to fire the laser, and to generate a pulse, which prepares the computer to read the incoming ADC output and to store the count in an appropriate channel. After 1.2 μs, a gating pulse of 1.7 μs width activates the ADC to start recording the total signal A. Since the laser repetition rate was 75 Hz, the time interval between two adjacent A gates is 12.5 ms. This interval is used to record the beam background by the B gate, which has the same width as the A gate and is generated approximately 1 ms after the immediately previous A

gate. Thus, the total signal and beam background are recorded

alternately in one half of the time used for a particular
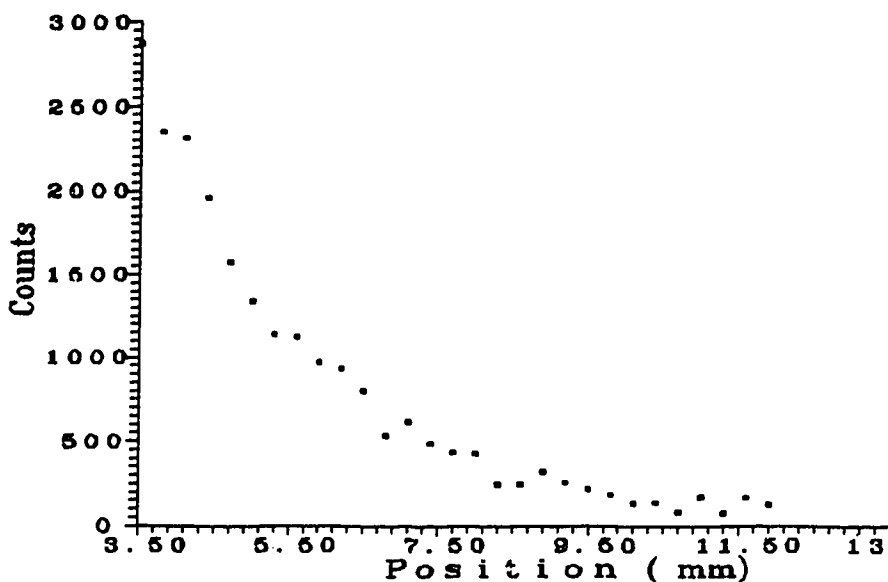
Fig.2.4-2 A typical decay curve for CrII
$z^6P_{3/2}$ level

data point. When this half time is over, the beam is blocked

and the laser background A' and the dark current B' are

recorded in the same way. The total time for measuring each

data point is 4 seconds in each sweep. The ion beam current is

recorded simultaneously during the same fixed time as A and B

to account for fluctuations. It is also digitized to be used

as a normalization for the final signal counts. Even so, the

beam current fluctuations are maintained as small as possible

to minimize possible errors. A typical decay curve is shown in

16

Fig(2.4-2).

2.5 Fitting the Decay Curve

Having obtained a decay curve, the lifetime can be derived accurately from it. The fluorescence signal decays exponentially with increasing distance from the excitation region. So, the lifetime can be obtained from a single exponential fitting.

A computer program written using the MATHCAD software package was designed to do this. In this program, data for each direction of motion (parallel or anti-parallel to the ion beam can be either analyzed separately or folded together. Before doing the analysis, the background must be subtracted from the total signal and the net signal must be normalized by the beam current. There are two methods to subtract the background. One is to subtract the laser background and the beam background directly from the total signal. For the ith data point, A_i, B_i and A_i' are the total signal, beam background and laser background respectively. The net signal is:

$$S_i = [A_i - B_i - A_i'] \frac{\overline{N}}{N_i} \qquad (2.5\text{-}1)$$

17

where N_i is the ith beam current count and N is the mean value of the beam current. The gated dark current is very small and is assumed to be zero.

The second method to correct for the background signals is to subtract a linear fitted background from the total signal. In this method the total background (laser background + beam background) is first fitted as a linear function of position:

$$Bg_i = m_1 x_i + b_1 \qquad (2.5\text{-}2)$$

where m_1 and b_1 are the fitted slope and intercept respectively. Therefore the net signal is:

$$S_i = [A_i - m_1 x_i - b_1]\frac{\overline{N}}{N_i} \qquad (2.5\text{-}3)$$

The net signal should be an exponential function of position, therefore:

$$S_i = A e^{-\alpha x_i}$$

$$\alpha = \frac{1}{v\tau} \qquad (2.5\text{-}4)$$

where A is the amplitude at X=0 and τ is the lifetime.

The coefficients A and α can be obtained using a weighted

least-squares fit to the linear equation:

$$Y_i = \ln S_i = \ln A - \alpha x_i \qquad (2.5-5)$$

The A_i, B_i and A_i' follow Poisson statistics[6][10], therefore the variance of the signal is:

$$Var(S_i) = [(A_i + B_i + A_i')\frac{\overline{N}}{N_i}]^{\frac{1}{2}} \qquad (2.5-6)$$

for the raw background and

$$Var(S_i) = [A_i \frac{\overline{N}}{N_i}]^{\frac{1}{2}} \qquad (2.5-7)$$

for the fitted background. The variance of Y_i is given by

$$Var(Y_i) = Var(\ln S_i) = \frac{Var(S_i)}{S_i} \qquad (2.5-8)$$

The data points are weighted in the fit as the inverse of the square of $Var(Y_i)$

$$W_i = \frac{1}{[Var(Y_i)]^2} \qquad (2.5-9)$$

The coefficient α can then be obtained:

19

$$\alpha = \frac{1}{\Delta} \begin{vmatrix} \sum_i W_i & \sum_i W_i Y_i \\ \sum_i W_i x_i & \sum_i W_i x_i^2 \end{vmatrix} \qquad (2.5\text{-}10)$$

where

$$\Delta = \begin{vmatrix} \sum_i W_i & \sum_i W_i x_i \\ \sum_i W_i x_i & \sum_i W_i x_i^2 \end{vmatrix} \qquad (2.5\text{-}11)$$

The fit itself gives the statistical error in the lifetime,

$$\delta\alpha = \frac{1}{\Delta} \sum_i W_i$$

$$\tau = \frac{1}{\alpha v} \qquad \cdot \qquad (2.5\text{-}13)$$

In order to test for a systematic variation of the lifetime, the points close to the interaction region are always truncated one at a time and the fit repeated. For each run, usually 4 to 5 points are truncated. The lifetime and the uncertainty are obtained from the weighted average of the values obtained from analysis using the various truncations. The goodness of fit is tested by calculating the reduced chi-square[6]:

20

$$\chi^2 = \frac{\sum_i W_i (Y_i - lnA + \alpha x_i)^2}{n-2} \qquad (2.5\text{-}14)$$

where n is the number of total data points.

Ideally, the square root of reduced chi-square is equal to 1, but in fact it is nearly always larger than 1, even though the data points distribute randomly on the both sides of the fitting curve. This reflects the difference between the estimated error for each data point and the real deviation, and suggests that the error in each data point is somewhat under-estimated in the analysis. Another possible reason for the root of reduced chi-square larger than 1 is that the number of photons being detected is slightly less than the actual value, which suggests that the charge-integration electronics may need to be recalibrated.

Weighting each individual lifetime measurement in terms of the uncertainty $\delta\tau$, the mean lifetime is obtained by:

$$\bar{\tau} = \frac{\sum_i \dfrac{\tau_i}{\delta\tau_i^2}}{\sum_i \dfrac{1}{\delta\tau_i^2}} \qquad (2.5\text{-}15)$$

The standard error of this mean is given by:

$$\delta\tau = \left(\cfrac{1}{\sum_i \cfrac{1}{\delta\tau_i^2}} \right)^{1/2} \qquad (2.5\text{-}16)$$

and the standard deviation in the lifetime value can be obtained by:

$$\delta\tau_{sd} = \left[\cfrac{n\sum_i [\frac{1}{\delta}\tau_i(\tau_i - \bar{\tau})]^2}{(n-1)\sum_i (\frac{1}{\delta\tau_i})^2} \right]^{1/2} \qquad (2.5\text{-}16)$$

The final uncertainty of the lifetime is taken as the larger of $\delta\tau$ and $\delta\tau_{sd}$. Details of this program can be found in Appendix I.

2.6 Sources of systematic Error

For beam-laser experiments, there are several possible sources of systematic error from different parts of the system. As mentioned earlier, the uncertainty of the beam velocity is one major source of systematic error. Although it is calibrated to better than 1% using the Doppler shift, it is still the most significant source of error. The second error source concerns the laser power variation. In most cases the laser power is not sufficient to completely saturate the

transitions excited, and hence the fluorescence signals are dependent on the laser power. As was analyzed in a previous thesis[19], a 1% laser power drop can cause 0.3% variation of the lifetime. The laser pulses were therefore monitored during the experiment by a photodiode to make sure that, for all data points, the laser radiation has the same average power. The total systematic error caused by the laser power variation is typically less than 1%.

CHAPTER THREE
LIFETIME MEASUREMENTS FOR MnII
AND CrII LEVELS

Lifetime measurements for the z^5P^o and z^7P^o levels in MnII and the $z^6P^o, z^6F^o, z^6D^o, z^4P^0$ and z^4D^o levels in CrII have been made by the beam-laser method. These results are presented and discussed in this chapter. The measurement for the $z^4D_{7/2}$ level of CrII is the first to be reported for that level.

3.1 Radiative lifetimes of MnII levels

The only levels of MnII which can be populated by the present experimental set up belong to z^5P^o and z^7P^o, because other levels are too high in energy to be reached by available laser wavelengths. The z^7P^o levels were populated from the ground state level, a^7S_3, using the dye Coumarin 500 and a BBO crystal. Population of the z^5P^o levels was achieved both from the ground state level, using Coumarin 460 and the BBO crystal, and from the first excited metastable state, a^5S_2, using Rhodamine 6G and a KDP crystal. The lower population of the a^5S_2 level, which has an energy of about 1.2 eV, was off-set by the larger probabilities for the a^5S to z^5P^o transitions. The decay curves obtained by using the two means of excitation gave a very similar number of peak counts per sweep. Because the a^5S_2 level is about 1.2 eV higher than the

24

ground state a^{7}S$_3$, the signal was naturally stronger from the z^{7}P^o levels than from the z^{5}P^o levels. Hence the lifetimes of the z^{7}P^o levels were measured with significantly better precision than were the z^{5}P^o levels. The beam current in the MnII experiment was typically 5 μA. Each level was measured at least five times and for each measurement successive sweeps were summed until the decay curve reached typically 2000 counts at the peak.
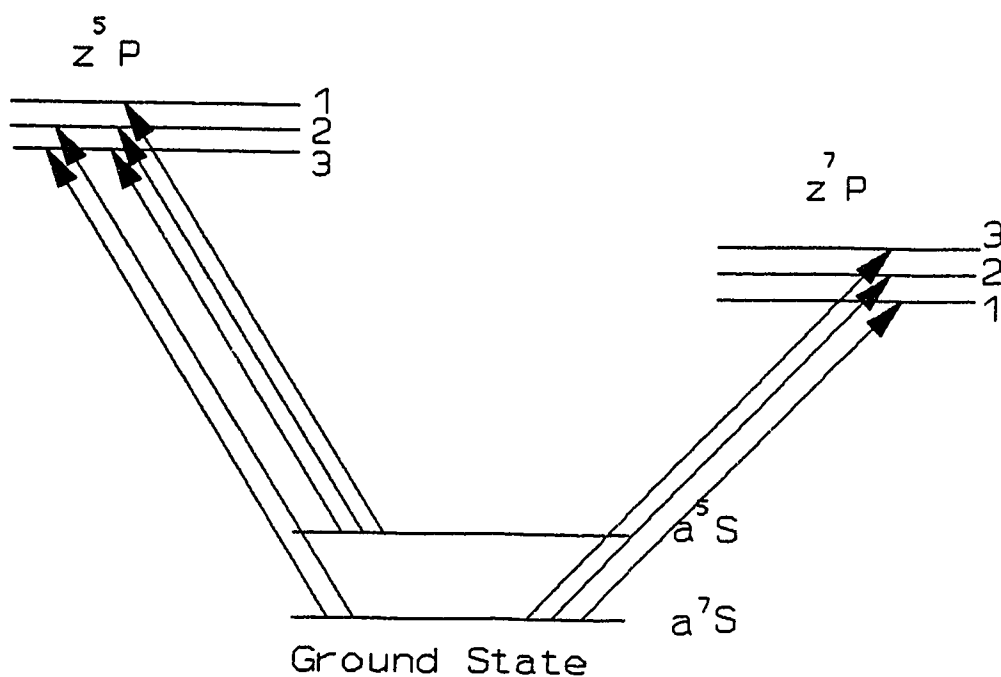
Fig 3.1-1 Excitation of MnII levels

The lifetimes of the z^{5}P^o and z^{7}P^o levels in MnII are listed in Table (3.1-1), where experimental uncertainties in the last digits are shown in parentheses. Previous measurements and

calculations are also listed in this table for comparison. The results of this work are in good agreement with previous laser-induced fluorescence measurements but have a higher precision[18]. In comparison with the calculations of Kurucz, the interesting thing is that his most recent calculations give results closer to experiment than do the earlier calculations for the z^7P^o levels but are in somewhat worse agreement with experiment for the z^5P^o levels. The gf-values calculated by Kurucz [16] are widely used for the calculations
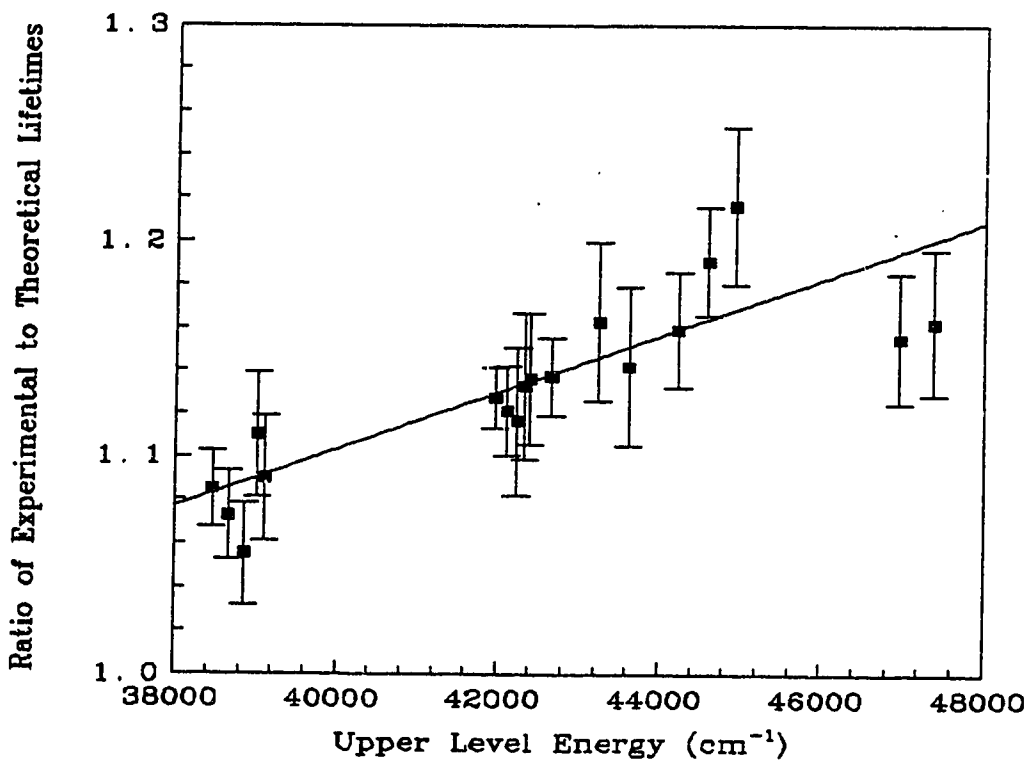
Fig 3.1-2   The ratio of experimental and theoretical
            lifetime against level energy in FeII [15]

of solar abundances. The difference between the experiment and the calculations by Kurucz for MnII indicates the gf-values calculated by Kurucz should be corrected, as should the solar manganese abundance obtained using his gf-values.
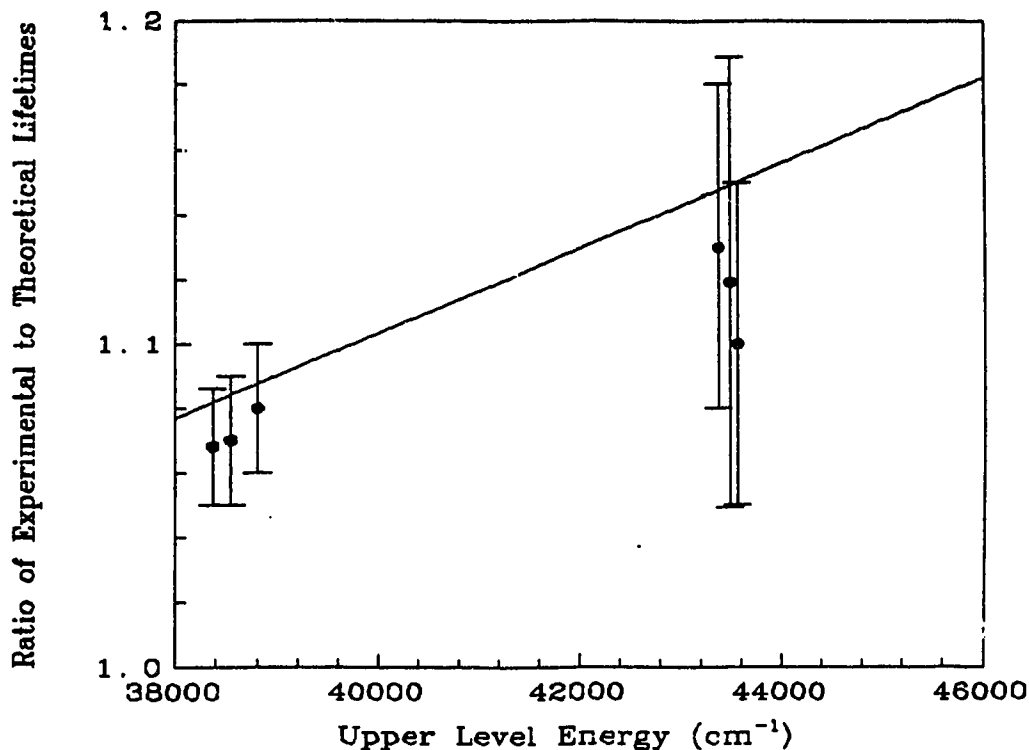
Fig 3.1-3 The ratio of experimental and theoretical
lifetimes against level energy for MnII

In the earlier measurements for low-lying quartet and sextet levels of FeII, a trend that shows the ratio of the experimental and the theoretical lifetimes as a function of level energy was found[15]. This trend is shown in Fig(3.1-2). A very similar dependence was found for the MnII data, as

shown in Fig(3.1-3), where the solid line is the line fitted to the FeII data (Fig 3.1-2). From the data of MnII and FeII we see that the ratio of measured lifetime to that calculated from Kurucz's gf-values appears to increase systematically with the energy of the levels involved. This empirical energy-dependent relation provides an important correction to Kurucz's gf-values for these ions.

Table 3.1-1   Lifetimes of MnII

Level	Excitation wavelength (nm)	Radiative Lifetimer (ns)				
		This work	A	B	C	D
z^5P_1	293.305	4.05 (10)	3.9(3)	5.3(5)	3.69	3.87
z^5P_2	293.930	4.15 (10)	4.1(3)	5.4(5)	3.69	3.87
z^5P_3	294.920	4.24 (10)	4.1(3)	4.4(4)	3.70	3.84
z^7P_2	260.570	3.66 (5)	3.7(4)	4.4(4)	3.42	3.06
z^7P_3	259.373	3.60 (5)	3.8(4)	4.7(5)	3.38	3.01
z^7P_4	257.611	3.54 (5)			3.30	2.96

A. Laser-induced fluorescence (Kwiatkowski et al 1982)
B. Beam-foil (Martinson et al 1973)
C. Semiempirical calculation (Kurucz 1988)
D. Semiempirical calculation (Kurucz and Peytremann 1975)

3.2 Radiative lifetime of CrII levels

The z^6F^o, z^6P^o, z^6D^o, and z^4P^o levels of CrII were populated from the first excited, metastable state, a^6D^o, which has an energy of 1.5 eV, using the dye Coumarine 540 and a KDP crystal for

z^{6}F°, and a mixture of dye Coumarine 540A and dye Coumarine 500 and a BBO crystal for z^{6}P°, z^{6}D° and z^{4}P°. Because the population of the a^{6}D° levels is very low, the signal obtained, even for strong transitions, is much lower than the signal obtained in the MnII experiments. The z^{4}D$_{7/2}$ level was populated from the second excited, metastable state, a^{4}D°, which has an energy about 2.4 eV. The population of this metastable state is lower than the first metastable state. In order to obtain a sufficient signal-to-noise ratio for the decay curves, the
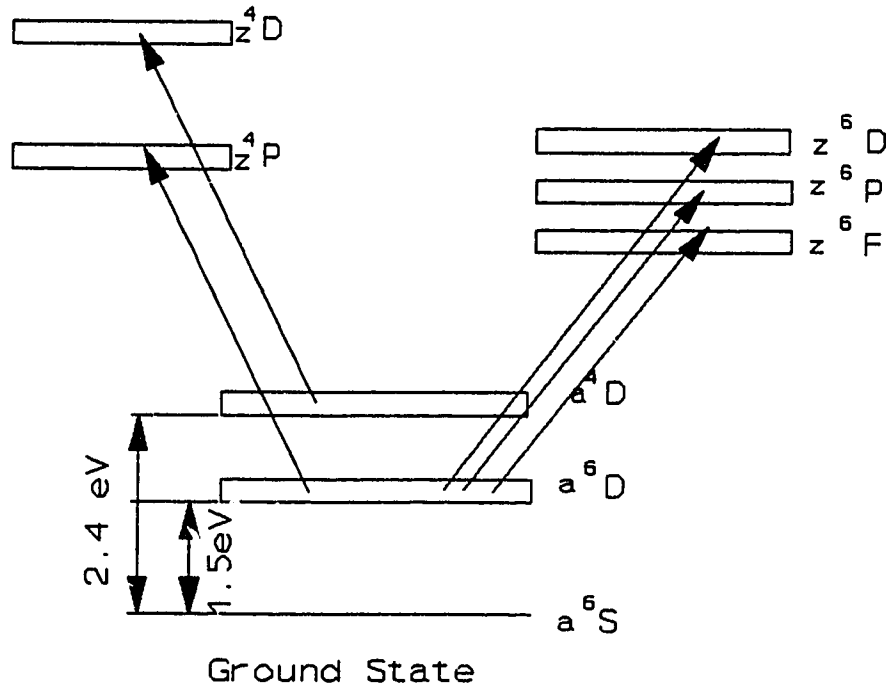
Fig.3.2-1 Excitation of CrII levels

experiments had to be run with a high beam current, typically from 8 to 10 μA. This is a big challenge for the ion source.

The beam current was usually not very stable at this current and the ion source filament was very easily broken. Another difficulty with the ion source in the CrII experiments was that the anode and the filament often became shorted during the experiment, and the ion source then had to be taken apart for cleaning even if the filament was not broken. In spite of these difficulties in the CrII experiments, each level was measured at least five times and the peak counts of each decay curve was accumulated to at least 1500. Because of the low population of the a^4D^o levels, the $z^4D^o_{7/2}$ lifetime measurements had a relatively low signal-to- noise ratio. Hence the precision of the lifetimes measured for this level is lower than for the other levels. However, this is the first reported measurement for this level. The lifetimes of the z^4D^o levels have astrophysical interest. Since most of the weak absorption lines of CrII found in solar photospheric spectra involve transitions in which the upper levels are low lying quartet levels, astrophysicists are more interested in the quartet levels in CrII than in the sextet levels.

The lifetimes of the CrII levels studied here are listed in Table(3.2-1), where they are compared with previous measurements and calculations. The results of this work are in good agreement with the measurements by Schade and have comparable precision[27]. Just as for the FeII and MnII data, the lifetimes from the CrII experiments are systematically

longer than the theoretical calculations by Kurucz. The ratio
of experimental and theoretical lifetimes against the level
energy is plotted as Fig(3.2-2). From Fig(3.2-2), we see that
the dependence on level energy is not as pronounced as it was
for FeII and MnII. It is interesting to note that the ratios
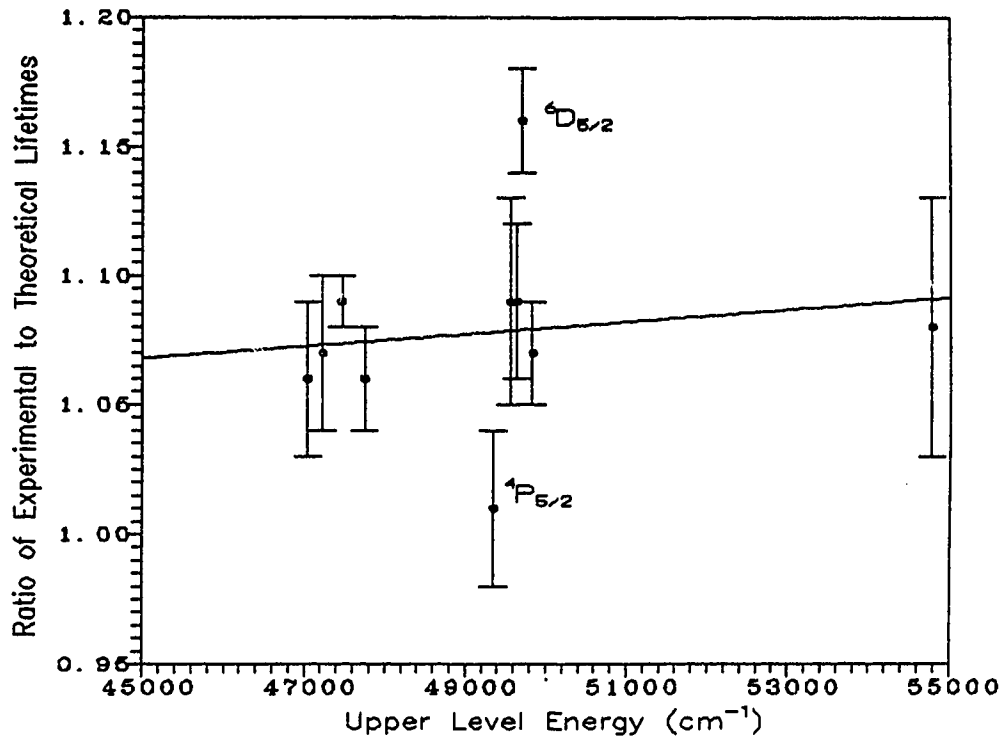
Fig.3.2-2 Theratio of experimental and theoretical
lifetimes against level energy for CrII

of experimental to theoretical lifetimes for the $z^4P_{5/2}$ and
$z^6D_{5/2}$ levels lie symmetrically about the fitted straight line.
It is known that these two levels interact strongly with each
other. From the lifetimes listed in Table 3.2-1, we see that
our result for $z^4P_{5/2}$ is quite different from the result

measured by Schade et al[26]. Different from other z^4P levels, the lifetime of this level is very close to the values of z^6D levels. The interesting thing is that the lifetime of $z^6D_{5/2}$ is

Table 3.2-1 Lifetimes of CrII

Level	Excitation wavelength (nm)	Radiative Lifetimes (ns)				
		This work	A	B	C	D
$z^6F_{11/2}$	283.563	4.14 (9)	4.0(1)	5.0(7)	3.3(3)	3.88
$z^6F_{9/2}$	284.324	4.29 (8)	4.2(1)			3.92
$z^6F_{7/2}$	284.938	4.29 (14)	4.1(1)			3.95
$z^6F_{5/2}$	286.510	4.21 (15)	4.2(1)	5.3(7)	4.2(2)	3.98
$z^6F_{3/2}$			4.2(1)	4.8(5)		4.00
$z^6D_{9/2}$	266.342	3.88 (5)	3.8(2)	5.1(7)	3.2(2)	3.65
$z^6D_{7/2}$	269.103	3.90 (13)	3.8(1)	5.1(7)		3.64
$z^6D_{5/2}$	267.283	4.52 (10)	4.5(1)	5.4(6)		3.92
$z^6D_{3/2}$	267.108	4.19 (6)	4.2(1)			3.83
$z^6P_{7/2}$	276.665	2.40 (13)	2.5(1)	3.3(4)		2.05
$z^6P_{5/2}$	276.258	2.45 (8)	2.5(1)	3.2(4)		2.09
$z^6P_{3/2}$			2.4(1)	3.3(6)		2.11
$z^4P_{5/2}$	269.840	4.27 (7)	4.6(2)	4.1(4)		4.26
$z^4P_{3/2}$	271.230	4.65 (11)	4.7(2)			4.33
$z^4P_{1/2}$	272.274	4.87 (12)	5.0(2)			4.74
$z^4D_{7/2}$	287.597	4.20 (18)				3.89

A. Laser-induced fluorescence (Schade et al 1990)[27]
B. Beam-foil (Engman et al 1975)[8]
C. Beam-foil (Pinnington et al 1973)[23]
D. Semiempirical Calculation (Kurucz 1988)[17]

also very close to the values of z^{4}P levels. The reason for this is not very clear. However, our results suggest that the interaction has been under-estimated in the Kurucz calculation.

3.3 Applications to Astrophysics

The most direct application of lifetime measurements is for the calculation of solar elemental abundances. These calculations are performed using the solar photospheric spectra and precise f-values. The equivalent widths of absorption lines in solar photospheric spectra can be obtained by integration of the line profiles. As shown in Fig(3.3-1), the equivalent width of an absorption line is defined as the width of a rectangular strip of height $I_\lambda(0)$ which has the same area as that of the absorption line. Therefore:

$$W_\lambda = \int [1 - \frac{I_\lambda(L)}{I_\lambda(0)}] d\lambda \qquad (3.3-1)$$

where I(0) and I(L) are the intensities of the incident and transmitted radiation respectively, and L is the length of the absorbing column. The intensity of the light transmitted through a non-radiating medium is given by:

$$I_\lambda(L) = I_\lambda(0)\exp(-\kappa_\lambda L)d\lambda \qquad\qquad (3.3\text{-}2)$$

where κ_λ is the absorption coefficient of the medium. Therefore the equivalent width can be written in terms of the absorption coefficient:

$$W_\lambda = \int [1 - \exp(-\kappa_\lambda L)]d\lambda \qquad\qquad (3.3\text{-}3)$$
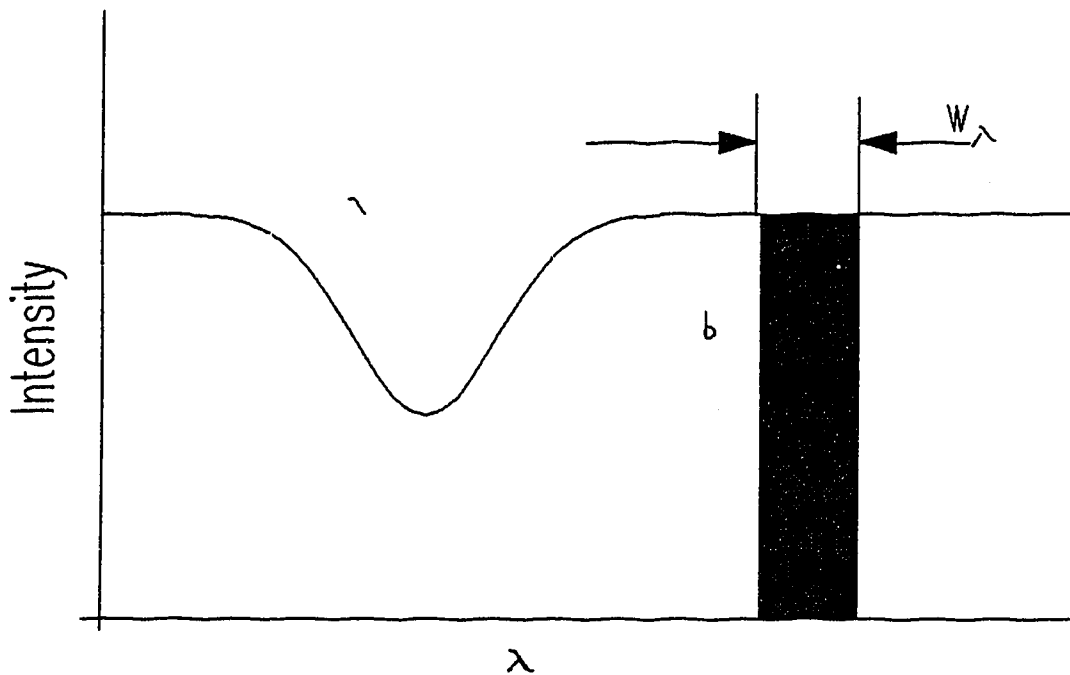
Fig.3.3-1 The equivalent width

For an optically-thin sample, $\kappa_\lambda L \ll 1$, at the absorption centre, the equivalent width then can be written[7]:

34

$$W_\lambda = \int \kappa_\lambda L d\lambda$$

$$= \frac{h\lambda_{ik}}{8\pi^2 c} B'_{ik} N_i L (1 - \frac{g_i N_k}{g_k N_i}) \int g(\lambda) d\lambda \qquad (3.3\text{-}4)$$

The integral in (3.3-4) is equal to unity since the line shape function $g(\lambda)$ is normalized. The ratio of level population in thermal equilibrium satisfies:

$$\frac{g_i N_k}{g_k N_i} = \exp(\frac{-h\upsilon_{ik}}{kT}) \qquad (3.3\text{-}5)$$

This ratio is very small for solar temperatures, and thus equation (3.3-4) can be reduced to:

$$W_\lambda = \frac{h\lambda_{ik}}{8\pi^2 c} B'_{ik} N_i L \qquad (3.3\text{-}6)$$

The relation between the coefficient, B_{ik}, and the oscillator strength, f_{ik}, is given by:

$$B'_{ik} = \frac{2\pi^2 e^2}{\varepsilon_0 m h \upsilon_{ik} c} f_{ik} \qquad (3.3\text{-}7)$$

Therefore the equivalent width finally can be written:

$$W_\lambda = \frac{\pi e^2 \lambda_{ik}^2}{4\pi\varepsilon_0 mc^2} f_{ik} N_i L \qquad (3.3\text{-}8)$$

35

In the optically thin case, the density of atoms in the lower level involved in the transition can be calculated from the equivalent width and the f-value.

When the condition $\kappa_\lambda L \ll 1$ is no longer valid, the complete expression for the equivalent width(3.3-3) must be used. It is a function of the product of the line λf-value and the density of atoms in the state from which absorption occurs. A graph of $\log(W_\lambda/\lambda)$ against $\log(\lambda f)$ is called the curve of growth[7], which is very important in the determination of solar elemental abundances. So far we have only considered absorption transitions with a common lower level, i. In most cases the lower levels of the lines involved in the curve of growth are different. Therefore a correction based on the Boltzmann distribution for each level to the ground state is necessary. With this correction, the equivalent widths for optically thin lines are given by:

$$W_\lambda = \frac{\pi e^2 \lambda_{ik}^2}{4\pi\varepsilon_0 mc^2} f_{ik} L [N_0 g_i / g_0 e^{-E/kT}] \qquad (3.3-9)$$

where g_0 and N_0 are the statistical weight and population of the ground state respectively. Therefore we have:

$$Log(\frac{W_\lambda}{\lambda})=\log(\lambda gf)-0.434(\frac{E_i}{kT})+constant \qquad (3.3-10)$$

Generally the curve of growth is plotted using a correction parameter X:

$$X=\lambda gfe^{-E/\mu T} \qquad (3.3-11)$$

A typical curve of growth for FeII in the solar atmosphere is shown in Fig(3.3-2), in which all levels are corrected to the ground state, and the λf-value is replaced by the correction parameter X. If the absorption is very weak (optically-thin), the relation between $\log(W_\lambda/\lambda)$ and $\log(X)$ gives the linear part of the curve with unit slope. In this case, if the element is limited to a single stage of ionization, and the lower level of the transition is the ground state, the solar abundance of that element can be calculated:

$$logA=\log\frac{NL}{N_H}=\log(\frac{W_\lambda}{\lambda})-\log\lambda f-logN_H+20.053 \qquad (3.3-12)$$

Here logA is the abundance of the element relative to hydrogen and N_H is the column density of hydrogen in the solar atmosphere ($logN_H$ is assumed to be 12). In the solar atmosphere, the element is not limited to one stage of
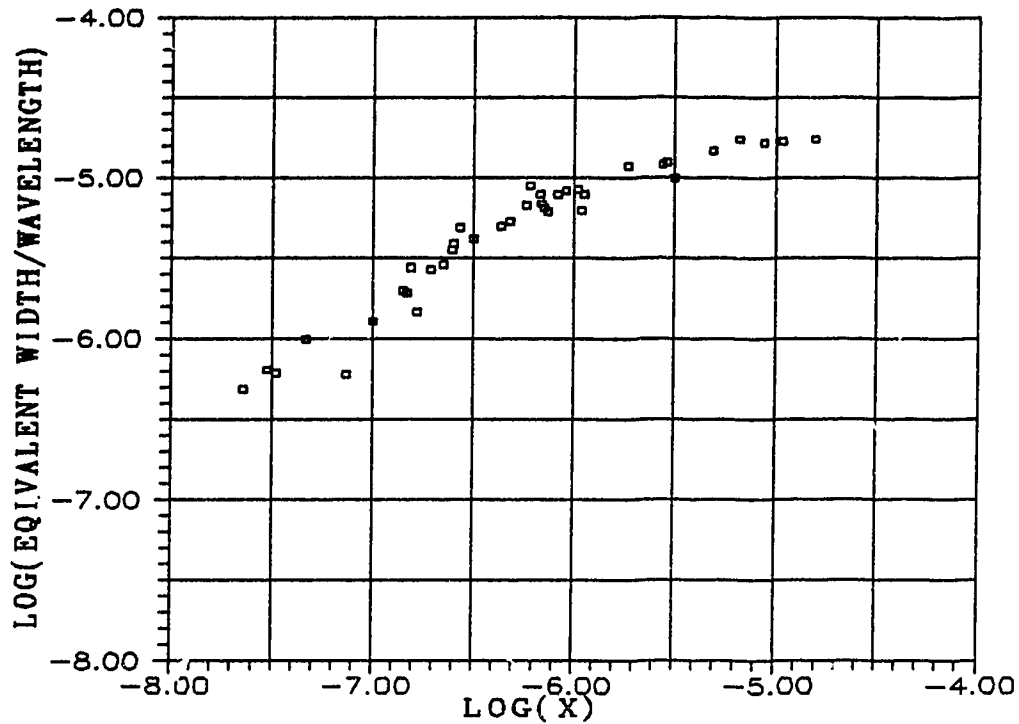
Fig.3.3-2 The curve of growth for FeII

ionization. The ratio of ions to neutrals in thermodynamic
equilibrium is a function of temperature given by the Saha
relation[14]:

$$\frac{N_{ion}N_e}{N_{neutrals}} = \phi(T) \qquad (3.3\text{-}13)$$

where N_e, $N_{neutral}$ and N_{ion} are column densities of electrons,
neutral atoms and ion atoms in the solar atmosphere. $\Phi(T)$ is

a function of temperature which depends on the model of the solar atmosphere. Hence the abundance of the element in the solar atmosphere can be calculated. For lines which are not in the linear part of the curve of growth, calculation of the solar abundance is still possible but more complicated. The abundance derived from such lines depends not only on the solar atmosphere model, but also on the values assumed for parameters required in the calculations, such as the line damping constant and the microturbulence velocity.

Fig(3.3-3) and Fig(3.3-4) show the curves of growth for MnII and CrII. The solar photospheric spectra data and the equivalent widths in these curves were analyzed and calculated by Dr.Biemont at the University of Liege[4][15]. In the case of MnII, the lifetimes of all six upper levels of the photospheric lines belonging to the z^5P and z^7P levels have been measured. None of these lines is in the linear part of the curve of growth. Hence the solar abundance analysis is dependent on details of the solar atmosphere, and the resulting uncertainty is relatively large, i.e. logMn=5.55±0.09[15]. This value includes a correction to the Kurucz gf-values based on our lifetime results. For CrII, most of the upper levels of the photospheric lines shown in Fig(3.3-4) are quartet levels[4], only a few lines involve sextet levels. Almost half of the lines are in the linear part of the curve of growth, and hence the solar chromium abundance

can be obtained directly from the f-values of these
transitions. Unfortunately, most of levels which can be
measured in our experiments belong to sextet states. As in the
other cases, calculations of the solar chromium abundance from
the level lifetimes rely on the branching ratios calculated by
Kurucz. However, the experimental lifetimes and the
theoretical lifetimes calculated by Kurucz's gf-values show a
systematic deviation of about 8%. Including this 8% correction
to Kurucz's gf-values gives a solar chromium abundance equal
to 5.69±0.04.
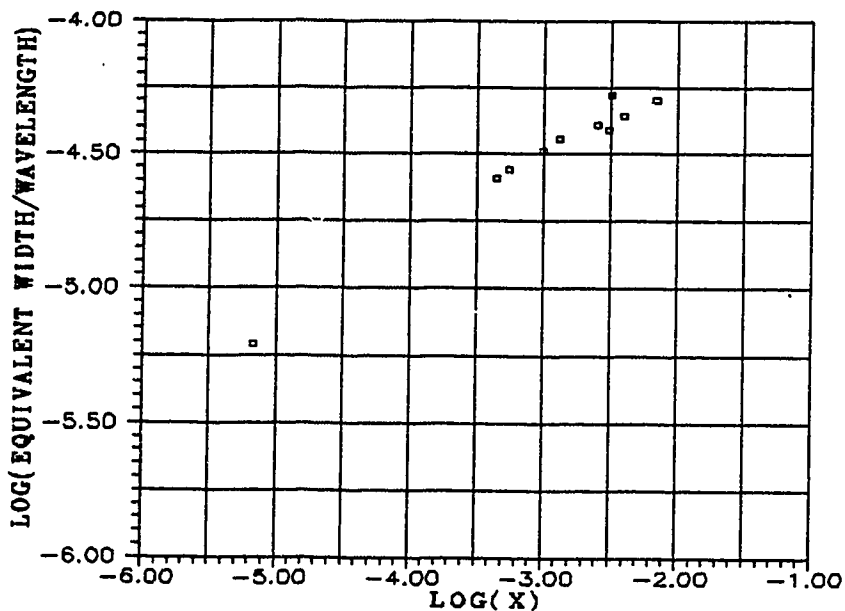
Fig.3.3-3 The curve of growth for MnII
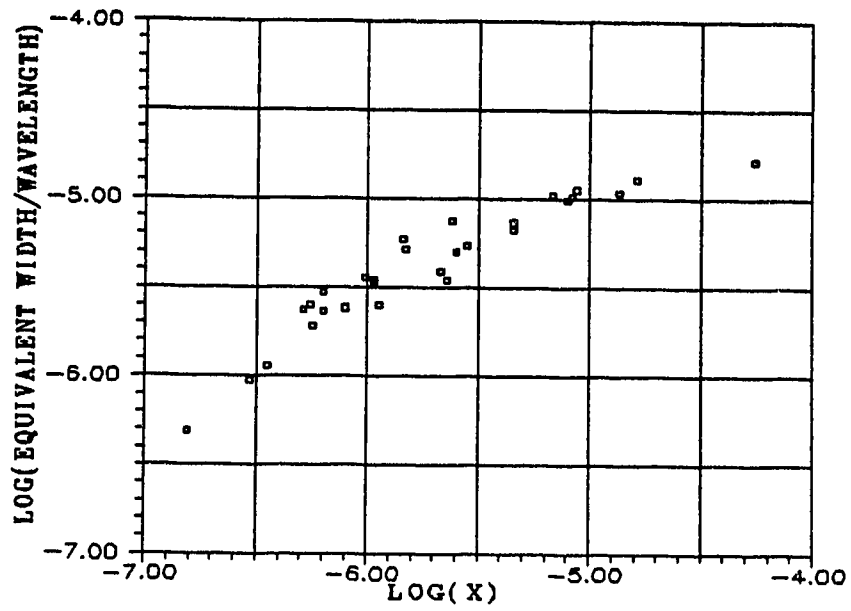
Fig.3.3-4 The curve of growth for CrII

Chapter Four

The Laser Excitation Process

for a Fast Beam

The excitation of a beam by laser radiation is a complicated process. The intensity of resonant fluorescence is dependent on how many atoms are excited to the upper level of the transition. This excitation process can not be described by the rate equations, because the atoms in the beam are subject to a very strong electromagnetic field and the Rabi frequency (discussed on page 49) related to this strong field is usually larger than the atomic natural frequency width[20]. In order to describe this process, a semiclassical theory must be used in which the atoms in the beam are treated by quantum mechanics and the radiation field is treated as a classical field. Before doing this, it is necessary to establish a system model and to have an order-of-magnitude estimate of some important parameters used in this calculation for our experimental arrangement.

The intensity of the laser radiation can be estimated from the average power and the repetition rate. The laser repetition rate used in this experiment is 75 Hz and the average power is generally 1 to 2 mW. In this calculation, we take a conservative estimate, 0.5 mW. The width of the laser pulse is about 5 ns. Therefore the average laser power during

each pulse is:

$$\bar{P} = \frac{0.5 \times 10^{-3}}{75 \times 5 \times 10^{-9}} = 1.33 kW$$

The laser spot size is about 0.14 cm^2, so the laser intensity is :

$$I = \frac{\bar{P}}{A} \approx 10 kW/cm^2$$

The laser radiation can be treated as a continuous wave during the time of interaction with the atoms in the beam, because the laser pulse duration is greater than the time an atom spends in the interaction region (usually less than 1 ns).The atomic lifetimes being measured (typically 4 to 5 ns) are significantly longer than the interaction time (1 ns). Therefore it is reasonable to assume that there is no decay during excitation.

Based on these estimates, we can use an isolated two level system without relaxation under the action of a CW electromagnetic field to describe the population process.

4.1 Two level model

Let us first consider a two level system, as shown in

43

Fig(4.1-1). For simplicity, we assume the statistical weights for the two levels are 1. The stationary wave functions for the state having energies E_1 and E_2 are $\psi_1(r)$ and $\psi_2(r)$ respectively. When a radiation field with frequency ω is applied to this system, the Hamiltonian can be written as:

$$H=H_0+H_1 \qquad (4.1-1)$$

———————————————— E_2

hv
——————➤

———————————————— E_1
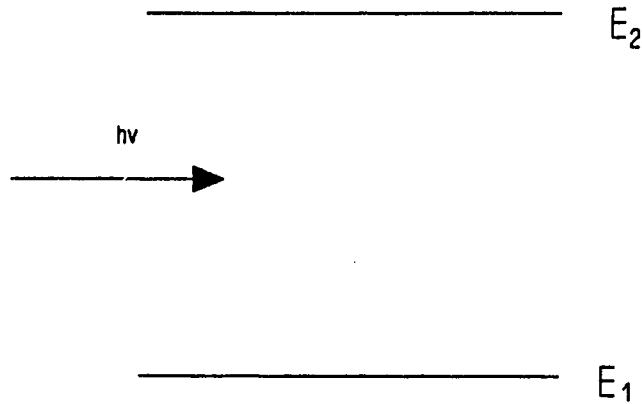
Fig.4.1-1 Two level system model

where H_0 is the stationary Hamiltonian and the electric dipole interaction Hamiltonian H_1 has the form:

$$H_1=-e\vec{E}\cdot\vec{r} \qquad (4.1-2)$$

where er is the electric dipole moment operator of a particle and E is the electric field strength of the wave.

44

The wave function of this time-dependent system satisfies the Schrödinger equation:

$$i\frac{h}{2\pi}\frac{\partial \Psi}{\partial t}=H\Psi \qquad (4.1-3)$$

and can be expanded by:

$$\Psi=a_1 e^{-i\frac{2\pi E_1}{h}t}\psi_1+a_2 e^{-i\frac{2\pi E_2}{h}t}\psi_2 \qquad (4.1-4)$$

where a_1 and a_2 are time-dependent coefficients. Substituting (4.1-4) in (4.1-3) gives:

$$i\frac{h}{2\pi}\frac{da_1}{dt}\psi_1 e^{-i\frac{2\pi E_1}{h}t}+i\frac{h}{2\pi}\frac{da_2}{dt}\psi_2 e^{-i\frac{2\pi E_2}{h}t}$$

$$=a_1 H_1\psi_1 e^{-i\frac{2\pi E_1}{h}t}+a_2 H_1\psi_2 e^{-i\frac{2\pi E_2}{h}t} \qquad (4.1-5)$$

Multiplying (4.1-5) by ψ_1^* and integrating over spatial variables, we have:

$$i\frac{h}{2\pi}\frac{da_2}{dt}e^{-i\frac{2\pi E_2}{h}t}=a_1 e^{-i\frac{2\pi E_2}{h}t}\int \psi_1^* H_1\psi_2 d^3r \qquad (4.1-6)$$

In the same way, multiplying by ψ_2^* , we get:

$$i\frac{h}{2\pi}\frac{da_1}{dt}e^{-i\frac{2\pi E_2}{h}t}=a_2e^{-i\frac{2\pi E_1}{h}t}\int\psi_2^*H_1\psi_1d^3r \qquad (4.1-7)$$

If the transition frequency ω_0 is:

$$\omega_0=\frac{2\pi(E_2-E_1)}{h} \qquad (4.1-8)$$

and the integration matrix element is given by:

$$V=\int\psi_1^*H_1\psi_2d^3r$$

$$V^*=\int\psi_2^*H_1\psi_1d^3r \qquad (4.1-9)$$

Eqs (4.1-6) and (4.1-7) take the form:

$$i\frac{h}{2\pi}\frac{da_1}{dt}=Va_2e^{-i\omega_0 t}$$

$$i\frac{h}{2\pi}\frac{da_2}{dt}=V^*a_1e^{i\omega_0 t} \qquad (4.1-10)$$

We assume that the electromagnetic field is a linearly polarized coherent travelling wave with frequency ψ and amplitude E_0, which is given by:

$$E=E_0\cos(\omega t-\vec{k}\cdot\vec{r})\vec{k} \qquad (4.1-11)$$

46

The wavelength of the radiation field is usually much greater than the atomic scale, therefore (4.1-11) can be written:

$$\vec{E} = E_0 \cos(\omega t) \vec{k} \qquad (4.1\text{-}12)$$

Therefore:

$$V = -\frac{1}{2} e E_0 (e^{i\omega t} + e^{-i\omega t}) \langle 1|z|2\rangle$$

$$V^* = -\frac{1}{2} e E_0 (e^{i\omega t} + e^{-\omega t}) \langle 2|z|1\rangle \qquad (4.1\text{-}13)$$

Let:

$$\tilde{V} = \frac{1}{2} e E_0 \langle 1|z|2\rangle$$

$$\tilde{V}^* = \frac{1}{2} e E_0 \langle 2|z|1\rangle \qquad (4.1\text{-}14)$$

So the equations (4.1-10) become:

$$i\frac{h}{2\pi}\frac{da_1}{dt} = -\tilde{V}[e^{i(\omega-\omega_0)t} + e^{-i(\omega+\omega_0)t}]a_2$$

$$i\frac{h}{2\pi}\frac{da_2}{dt} = -\tilde{V}^*[e^{i(\omega+\omega_0)t} + e^{-i(\omega-\omega_0)t}]a_1 \qquad (4.1\text{-}15)$$

The terms with the frequency $(\omega+\omega_0)$ on the right sides of (4.1-15) can be ignored because they oscillate very rapidly

47

and give a time average of zero. Hence the equations (4.1-14) reduce to a simpler form:

$$i\frac{h}{2\pi}\frac{da_1}{dt} = -\bar{V}a_2\exp(i\Omega t)$$

$$i\frac{h}{2\pi}\frac{da_2}{dt} = -\bar{V}^* a_1\exp(-i\Omega t) \qquad (4.1-16)$$

where:

$$\Omega = \omega - \omega_0$$

Before the radiation field is applied to this system, the system is in the lower energy level E_1. Therefore, at t=0

$$|a_1(0)|^2 = 1 \quad , \quad |a_2(0)|^2 = 0 \qquad (4.1-17)$$

and because this system has no relaxation during the interaction time, the total probability is conserved. Therefore:

$$|a_1(0)|^2 + |a_2(0)|^2 = 1 \qquad (4.1-18)$$

The solution of equation (4.1-16) with initial conditions (4.1-17) and (4.1-18) can be obtained (see Appendix II for details) and therefore the probability of finding the system in level E_2 at time t is:

$$P(t) = |a_2(t)|^2$$

$$= \frac{2(\frac{2\pi \tilde{V}}{h})^2}{\Omega^2 + (\frac{4\pi \tilde{V}}{h})^2}(1 - \cos[(\Omega^2 + (2\frac{\tilde{V}}{h})^2)^{1/2}t]) \quad (4.1\text{-}19)$$

If there is a total of N atoms in this system, at time t the number of atoms in the upper level is:

$$N_2(t) = \frac{2N\frac{2\pi \tilde{V}^2}{h}}{\Omega^2 + (\frac{4\pi \tilde{V}}{h})^2}(1 - \cos((\Omega^2 + (\frac{4\pi \tilde{V}}{h})^2)^{1/2}t) \quad (4.1\text{-}20)$$

The number of atoms in the upper level is oscillating with time as shown in Fig(4.1-2). The frequency of this oscillation is called the Rabi frequency[26]:

$$\omega_R = \sqrt{\Omega^2 + (\frac{4\pi \tilde{V}}{h})^2} \quad (4.1\text{-}21)$$

which is dependent on the intensity of the laser radiation.

4.2 Saturated Excitation

Using the Eq.(4.1-20), we can make an estimate of the laser intensity for saturated excitation. We know that the maximum
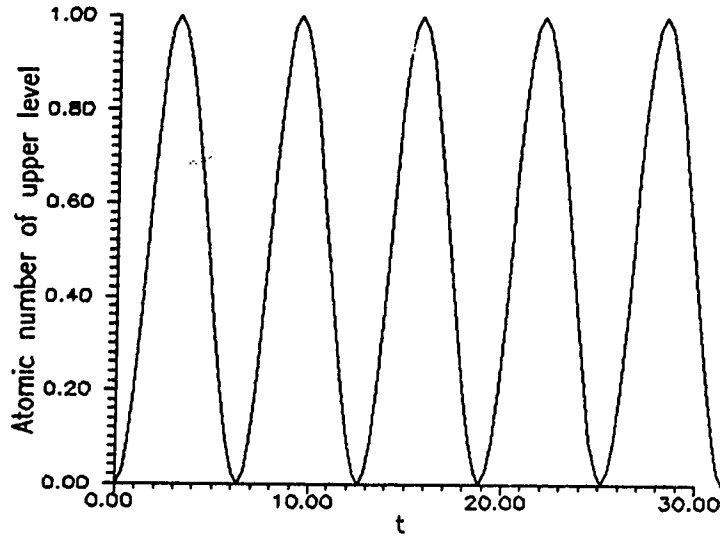
Fig.4.1-2 The number of atom in upper level
oscillates at the Rabi frequency

interaction time of the atoms with the laser is about 1 ns and
the excitations for different pulses are not phase related.
Therefore the number of atoms being excited to the upper level
is the time average over the maximum interaction time τ_i.

$$\overline{N_2} = \frac{1}{\tau_i} \int_0^{\tau_i} N_2(t)dt$$

$$= \frac{2N(\frac{2\pi \tilde{V}}{h})^2}{\Omega^2 + (\frac{4\pi \tilde{V}}{h})^2} (1 - \frac{1}{\tau_i} \int_0^{\tau_i} \cos(\omega_R t)dt) \qquad (4.2-1)$$

50

If $\tau_i \gg 2\pi/\omega_R$, we have:

$$\overline{N_2} = \frac{1}{2} N \qquad (4.2\text{-}2)$$

This is saturation. So the condition for saturated excitation is:

$$\tau_l \gg \frac{2\pi}{\omega_R} \qquad (4.2\text{-}3)$$

The Rabi frequency at $\Omega=0$ can be expressed as:

$$\omega_R = \sqrt{\Omega^2 + \left(\frac{4\pi\tilde{V}}{h}\right)^2} = \frac{|4\pi\tilde{V}|}{h} \qquad (4.2\text{-}4)$$

and

$$|\tilde{V}| = \frac{1}{2} eE_0 |{<}1|z|2{>}| \qquad (4.2\text{-}5)$$

We know that[20]:

$$I_0 = \frac{1}{2}\varepsilon_0 c E_0^2 \qquad (4.2\text{-}6)$$

$$|{<}1|z|2{>}|^2 = \frac{3\varepsilon_0 h C^3}{2\pi e^2 \omega_0^3} A_{21} \qquad (4.2\text{-}7)$$

Therefore the Rabi frequency can be written:

$$\omega_R = \frac{|4\pi \bar{V}|}{h} = 2\sqrt{\frac{6\pi^2 c^2 A_{21} I_0}{2h\omega_0^3}} \qquad (4.2-8)$$

The intensity requirement for saturation excitation is:

$$I_0 >> \frac{32\pi h\omega_0^3}{3c^2 A_{21}\tau_i^2} = I_s \qquad (4.2-9)$$

Using typical values in this experiment:

$$\omega_0 = 7.25 \times 10^{15} rad/s \,, \tau_{int} = 1ns, \ A_{21} = 0.5 \times 10^9 s^{-1}$$

the value of I_s can be calculated:

$$I_s = 7.49 \times 10^2 W/cm^2 \qquad (4.2-10)$$

Comparision with the laser intensity estimated in this experiment($^-$10kW), the saturation condition is generally satisfied. From (4.2-1) we see that the average number of atoms excited to the upper level is still dependent on the laser intensity when the detuning Ω is not zero, even if the saturation condition is satisfied. So this suggests that the laser frequency should be set as close to the line center as possible in the experiment.

When the beam and the laser intensity are stable, the line shape for resonant fluorescence is observed to follow the Lorentz distribution, because the fluorescence intensity is proportional to the number of atoms in the upper level of the transition. The line width of resonant fluorescence is also dependent on the intensity of laser radiation and the transition probability.

Chapter Five

Conclusion

5.1 Conclusion

By taking advantage of modern techniques, such as laser and non-linear optics, fast atomic beams and computers, the beam-laser technique is currently the most effective and accurate method for measuring atomic lifetimes. Compared with the beam-foil method, the beam-laser technique overcomes the cascading problem associated with the beam foil method and at the same time keeps the advantage of high time resolution. Because the beam-laser method is based on achieving the fluorescence from the level of interest by laser radiation, it is limited by the small fraction of levels which can be populated by laser radiation. In the experiments described in this thesis, single-step excitation has been used, and therefore the highest level energy which can be achieved by the shortest available laser wavelength (about 220 nm) is 5.6 eV above the ground state. Most of the higher excited levels can not be measured. Although some of the levels can be populated from low-lying metastable states, the low populations of these metastable states limits the signal-to-noise ratios so severely that, in most cases, the measurement can not be done.

Future development of the beam-laser method should

therefore be directed towards the excitation of higher energy levels. There are two possible methods. The first is to develop new sources of laser radiation at shorter wavelengths than are presently available. The use of the type A BBO crystal, which has become available recently, should lead to laser radiation with wavelengths down to 208 nm. If this laser radiation can be used in beam-laser experiments, the highest energy level which could be excited would be at about 6.0 eV above the ground state, and then a few more of levels of interest could be measured. The second possibility, which is more general and more complicated, is to use two-step or multi-step excitation. In this method, two or more laser radiations are used. The atoms in the beam are first pumped from the ground or low-lying state to an intermediate state by one laser and then excited to the level of interest by the second laser. Compared with one-step excitation, multi-step excitation can, in principle, excite most levels of interest, but is much more difficult to realize technically. To date, there are no reported measurements using this technique except for a specialized case[1] studied in this laboratory, in which two-step excitation was achieved using a single laser.

The beam-laser method can provide reliable lifetime results for the gf-value determinations and solar abundance calculations. The application of the results presented in this thesis to the solar elemental abundance calculations has given

improved solar manganese and chromium abundances.

Laser excitation of a fast beam is an important and complicated process. The importance of studying this process lies in the detern inon of the condition for saturated excitation. From ation presented in this thesis, we know that the are saturated under the conditions of laser intensity used here or some transitions that have relatively larger probabilities but, for many transitions that have small probabilities, the excitations are not saturated. Saturated excitation is very important for the beam-laser technique to have a high precision, because only under the condition of saturated excitation is the intensity of resonant fluorescence independent of variations of the laser intensity.

References

[1] W.Ansbacher, Y.Li, E.H.Pinnington, Phys.Lett. **139**, 165 (1989)

[2] S.Bashkin,ed., "Beam-foil Spectroscopy" J.Opt.Soc.Am. **61**, 1686 (1971)

[3] E.Biemont, M.Baudoux, R.L.Kurucz, W.Ansbacher and E.H.Pinnington, Astron. Astrophys. **249**, 539 (1991)

[4] E.Biemont, Mon. Not. Roy. Astron. Soc. **184**, 683 (1978)

[5] N.B.Delone, V.P.Krainov "Atoms in Strong Light Fields" Spring-Verlag,Berlin (1978)

[6] P.R.Bevington,"Data Reduction and Error Analysis for the Physical Sciences", McGraw-Hill, New York (1965)

[7] A. Corney,"Atomic and Laser Spectroscopy", Clarendon Press,Oxford (1983)

[8] B.Engman, A.Gaupp, L.J.Curtis, and I.Martinson, Phys. Scr. **12**, 220 (1975)

[9] A.Gaupp, P.Kuske and H.J.Andrä, Phys.Rev. **A26**, 3351 (1982)

[10] R.N.Gosselin,Ph.D Thesis, Univ.of Alberta,Edmonton (1988)

[12] R.N.Gosselin, E.H.Pinnington and W.Ansbacher, Nuclear Instruments and Methods in Physics Research **B31**, 305-309, North-Holland, Amsterdam.(1988)

[13] R.N.Gosselin, E.H.Pinnington and W.Ansbacher, Phys. Rev. **A38**, 4887 (1988)

[14] N.B.Gray, "The Observation and Analysis of Stellar

Photospheres", John Wiley and Sons, New York (1976)

[15] B.Guo, W.Ansbacher, E.H.Pinnington, Q.Ji and R.W.Berends, Phys.Rev. **A46**, 641,(1992)

[16] R.L.Kurucz and E.Peytremann, Smithsonian Astrophysical Observatory Special Report (1975)

[17] R.L.Kurucz, in Transactions of the International Astronomical Union, edited by M.McNally, **Vol.XXB.**(1988)

[18] M.Kwiatkowski, G.Micali, K.Werner and P.Zimmermann J.Phys.B:At.Mol.Phys. **15**, 4357 (1982)

[19] Y.Li, M.Sc thesis, Univ. of Alberta, Edmonton (1990)

[20] R. Loudon, "The Quantum Theory of Light", Clarendon Press, Oxford (1983)

[21] I.Martinson, in Proceedings of the Second European Conference on Beam-foil Spectroscopy, Lyon, July,1973

[22] H.Nubbemeyer, J.Quant.Spectrsc.Radiat.Trandfer. **16**, 396 (1976)

[23] E.H.Pinnington, and H.O.Lutz, Nuclear Instruments and Methods **110** (1973)

[24] E.H.Pinnington, B.Guo, Q.Ji, R.W.Berends, W.Ansbacher and E.Biemont, J.Phys.B:At.Mol.Phys. **25**, L475 (1992)

[25] R.C.Preston, J.Quant.Spectrosc. Radiat.Transfer **18**, 395 (1976)

[26] I.I.Rabi, Phys.Rev. **51**, 652 (1937)

[27] W.Schade, B.Mondt, and V.Helbig, Phys.Rev. **A42**, 1454 (1990)

Appendix I

Data Analysis

Analysis of the decay curve data obtained from these beam-laser experiments is performed by a program called "laserfit", which is written using the MATHCAD software package for a PC 286 computer. The basic principle of this program has been introduced in Chapter 2. Here I just discuss how to use this program to derive the lifetime.

Data Format

The decay curve data is recorded by the TN-11 computer. After being transferred to the PC computer, the data set has eight columns, which correspond to the distance, net signal (subtracted directly from the background), the laser background, total signal, beam background, beam current, ungated beam background and total number of laser pulses. The title of the data set has information about the element being measured, the beam energy, beam velocity, the repetition rate, the excitation laser wavelength, data set number, number of data points and number of sweeps. A typical data set is listed in the following table.

TABLE: A TYPICAL DATA SET

CR92 290 1.036 1 IQ 75.0 0.0 2722 5 58 4 11 112D

59

350	297	101	540	141	30304	46853	600
400	357	83	581	141	30409	47277	600
450	368	62	574	145	30192	47007	600
500	325	50	490	115	30206	47327	600
550	263	94	508	152	30405	47526	600
600	238	57	424	129	30268	47207	600
650	237	63	411	110	29765	46834	600
700	184	75	374	116	29769	47177	600
750	135	80	373	158	29586	46779	600
800	190	67	385	126	29875	47320	600
850	152	76	360	133	29750	47208	6)0
900	140	60	322	122	29490	46789	600
950	141	56	323.	126	29487	46780	600
1000	86	53	282	143	29383	46632	600
1050	48	54	252	149	29222	46569	600
1100	93	85	324	146	29400	46795	600
1150	121	75	311	114	29097	46204	600
1200	82	72	267	113	28830	46073	600
1250	90	73	280	115	29253	46582	600
1300	101	62	269	106	29206	46490	600
1350	19	70	224	135	28866	45985	600
1400	62	49	243	133	29028	45844	600
1450	64	67	259	130	28769	45840	600
1500	36	75	221	111	28670	46007	600
1550	31	54	242	157	28466	45757	600

1600	59	47	236	131	28608	45765	600
1650	24	75	214	11	28001	44971	600
1700	27	76	216	114	28358	45540	600
1750	41	44	213	129	28096	45143	600
1750	20	59	216	136	282.3	45634	600
1700	25	54	175	95	27973	45737	600
1650	26	50	183	107	27476	44968	600
1600	13	54	199	131	27234	44488	600
1550	34	90	226	102	26396	43219	600
1500	45	46	221	131	26810	43928	600
1450	40	71	215	104	26908	44022	600
1400	97	42	256	116	26814	43894	600
1350	66	49	237	123	26586	43644	600
1300	76	54	241	111	26651	43639	600
1250	110	47	265	107	27132	44343	600
1200	55	51	223	116	26615	43575	600
1150	61	67	245	117	27282	44655	600
1100	70	63	259	126	26283	43112	600
1050	96	52	292	144	27261	44526	600
1000	44	75	253	134	27606	45113	600
950	126	44	300	130	28082	45812	600
900	147	72	331	111	27999	45831	600
850	106	62	308	140	27952	45652	600
800	117	67	317	131	27960	45667	600
750	194	63	360	106	27312	44786	600
700	204	52	403	147	27519	45126	600

61

650	232	56	412	123	27515	45136	600
600	157	65	376	156	26252	43418	600
550	190	51	364	124	27159	44464	600
500	195	77	406	135	27133	44590	600
450	248	63	461	150	26585	43947	600
400	356	65	539	118	26834	44142	600
350	232	71	457	154	25492	42255	600

Program for data analysis

The program for decay curve analysis is composed of two major parts. One is called "laserfit", by which the data set can be read, displayed on the computer screen, truncated and fitted to an exponential function. The lifetime can be derived from this program. As mentioned in Chapter 2 , the data set is usually truncated 4-5 points from the front and refitted. The lifetimes from these truncations, combined with information concerning the uncertainties and reduced chi-squares, are output to a temporary file. In the "User-Defined-Parameters" part, the user can chose to analyze the data separately by each half or folded together, to subtract a raw background (subtract background directly) or a fitted background from the total signal. The point from which the truncation is performed can also be chosen from this part of the program. This is listed at the end of this Appendix as Program 1.

The second program is called "wtmean", by which the weighted average lifetime and statistical error can be calculated from the temporary file output from the "laserfit" program. This is listed as Program 2.

Batch File

The two programs mentioned above are run by a batch file written using DOS commands. Because the format of the data file transferred from the TN-11 computer can't be read directly by the "laserfit" program, the title of the data file must be deleted. So the first thing for this batch file to do is to read the data file from the diskette to a temporary file and to delete the title. The second function for this batch file is to link the two main programs. The thi: . function is to delete all the temporary file after the data analysis is finished. This batch file is listed in Prog.3

PROGRAM 1 LASERFIT

WEIGHTED POLYNOMIAL LEAST-SQUARES FIT

choose degree of polynomial to fit: D := 1

enter name of data file: $A := READPRN\begin{bmatrix}laser_{dat}\end{bmatrix}$

d := 0 ..D   N := rows(A)   N = 58

USER-DEFINED PARAMETERS:

startpt := 0   endpt := 28   (numbers between 0 and (N/2) - 1
                                if fold = 1; between 0 and N - 1
                                if fold = 0)

fit := 1   velocity := 1.039   (fit = 0: raw background;
                                  fit = 1: fitted background)

fold := 1   (fold = 1: folded data; fold = 0: unfolded data)

---

numpoints := endpt - startpt + 1

i := 0 ..numpoints - 1

$$pos_i := A^{<0>}_{i+startpt} - A^{<0>}_0$$

$$totsig_i := if\left[fold \approx 1, A^{<3>}_{i+startpt} + A^{<3>}_{N-startpt-i-1}, A^{<3>}_{i+startpt}\right]$$

$$laserbg_i := if\left[fold \approx 1, A^{<2>}_{i+startpt} + A^{<2>}_{N-startpt-i-1}, A^{<2>}_{i+startpt}\right]$$

$$beambg_i := if\left[fold \approx 1, A^{<4>}_{i+startpt} + A^{<4>}_{N-startpt-i-1}, A^{<4>}_{i+startpt}\right]$$

$$current_i := if\left[fold \approx 1, A^{<5>}_{i+startpt} + A^{<5>}_{N-startpt-i-1}, A^{<5>}_{i+startpt}\right]$$

background := laserbg + beambg

I := mean(current)

ml := slope(pos,background)   bl := intercept(pos,background)

$$bgchi := \sqrt{\sum_i \frac{\left[background_i - \left[ml \cdot pos_i + bl\right]\right]^2}{background_i}}$$

$$bgrechi := \frac{bgchi}{\sqrt{numpoints - 2}}$$

$$ns_i := if\left[fit \approx 0, totsig_i - background_i, totsig_i - ml \cdot pos_i - bl\right]$$

$$netsig_i := if\left[ns_i \le 0, 0.5, ns_i \cdot \left[\frac{I}{current_i}\right]\right]$$

$$varsig_i := if\left[fit \approx 0, totsig_i + background_i, totsig_i\right]$$

$$variable_i := ln\left[netsig_i\right]$$

$$sqrtwt_i := \frac{netsig_i}{\sqrt{varsig_i}} \qquad wtvar_i := sqrtwt_i \cdot variable_i$$

$$X^{<d>} := \overrightarrow{\left[sqrtwt \cdot pos^d\right]} \qquad coeff := (X^T \cdot X)^{-1} \cdot (X^T \cdot wtvar)$$

$$error_d := \sqrt{\left[(X^T \cdot X)^{-1}\right]_{d,d}}$$

$$f(t) := \sum_d coeff_d \cdot t^d \qquad Lifetime := -\left[100 \cdot velocity \cdot coeff_1\right]^{-1}$$

$$LifeError := \frac{-Lifetime}{coeff_1} \cdot error_1 \qquad z_i := sqrtwt_i \cdot \left[variable_i - f\left[pos_i\right]\right]$$

65

$$\text{chi} := \sqrt{\sum_i z_i^2} \qquad\qquad \text{reducedchi} := \frac{\text{chi}}{\sqrt{\text{numpoints} - 2}}$$

Plots   (Data points: +)   Number of points: numpoints = 29

$$\text{background}_i, m1 \cdot \text{pos}_i + b1$$
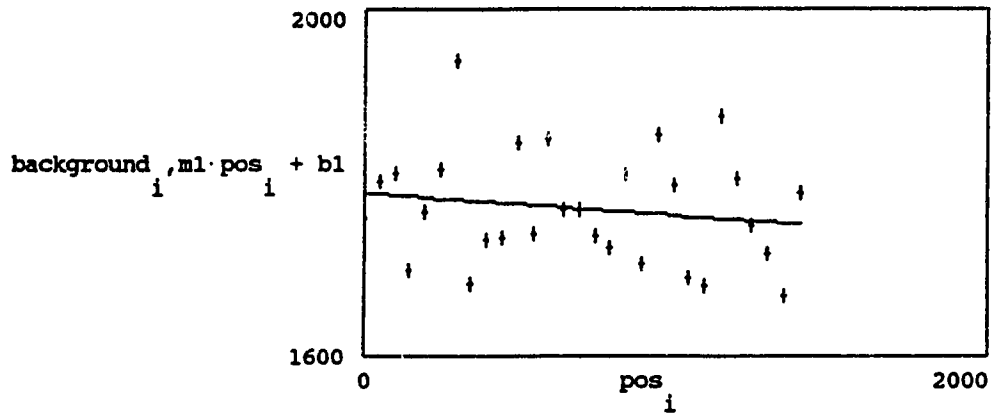
m1 = -0.0259   b1 = 1787.82069

bgchi^2 = 63.19244 bgrechi^2 = 2.34046

Coefficients of x^d and their errors:

d	coeff_d	error_d
0	8.4065	0.00947
1	-0.0021	0.00002

$$\text{variable}_i, f[\text{pos}_i]$$
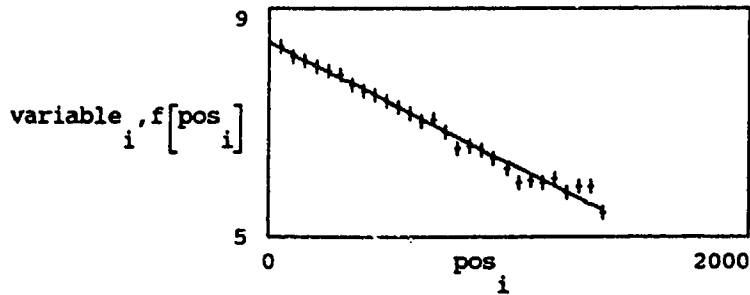
numpoints = 29

Lifetime = 4.5920

LifeError = 0.053

Residual plot: numpoints = 29
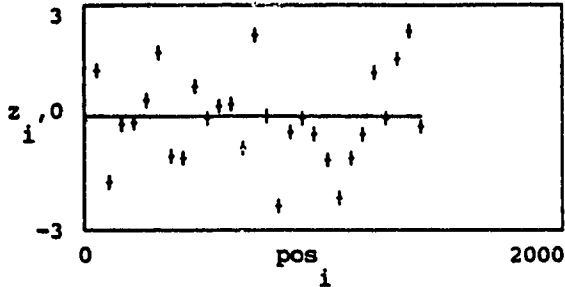
$$chi^2 = 38.82815$$

$$reducedchi^2 = 1.43808$$

out put the result to a file decaydat.prn

$R_{0,0} := reducedchi^2$ $R_{0,1} := chi^2$

$R_{0,2} := fit$ $R_{0,3} := fold$

$R_{0,4} := numpoints$ $R_{0,5} := 0$

$R_{1,0} := Lifetime$ $R_{1,1} := e^{coeff_0}$

$R_{1,2} := bl$ $R_{1,3} := bgrechi^2$

$R_{1,4} := startpt$ $R_{1,5} := 0$

$R_{2,0} := LifeError$ $R_{2,1} := R_{1,1} \cdot error_0$

$R_{2,2} := ml$ $R_{2,3} := bgchi^2$

$R_{2,4} := endpt$ $R_{2,5} := velocity$

$$R = \begin{bmatrix} 1.43808 & 38.82815 & 1 & 1 & 29 & 0 \\ 4.59201 & 4476.06045 & 1787.82069 & 2.34046 & 0 & 0 \\ 0.05385 & 42.3981 & -0.0259 & 63.19244 & 28 & 1.039 \end{bmatrix}$$

67

PROGRAM 2   WTMEAN

Input the Lifetime(T), LifeError(DT), and reduced chi square(chi)

$$A := \text{READPRN}\begin{bmatrix} \text{mean} \\ \quad \text{dat} \end{bmatrix}$$

$$T := A^{<0>} \qquad DT := A^{<1>} \qquad chi := A^{<2>}$$

$$N := \text{rows}(T) \qquad N = 4$$

$$invwt := \overrightarrow{\left[DT^2 \cdot chi\right]} \qquad wt := \overrightarrow{\left[\dfrac{1}{invwt}\right]}$$

$$\text{Lifetime} := \left[\dfrac{\overrightarrow{\Sigma(wt \cdot T)}}{\Sigma(wt)}\right] \qquad s_1 := \sqrt{\dfrac{N}{\Sigma(wt)}}$$

$$\text{samvar} := \left[\dfrac{N}{N-1}\right] \cdot \left[\dfrac{\overrightarrow{\Sigma\left[(wt) \cdot T^2\right]}}{\Sigma(wt)} - \text{Lifetime}^2\right]$$

$$s_2 := \sqrt{\text{samvar}} \qquad\qquad s_2 = 0.02089$$

$$\text{LifeError} := \max(s) \qquad\qquad s_1 = 0.07446$$

Lifetime = 4.5991   LifeError = 0.07446

$$T = \begin{bmatrix} 4.592 \\ 4.593 \\ 4.633 \\ 4.582 \end{bmatrix} \qquad DT = \begin{bmatrix} 0.05385 \\ 0.05913 \\ 0.06643 \\ 0.0714 \end{bmatrix} \qquad chi = \begin{bmatrix} 1.438 \\ 1.504 \\ 1.473 \\ 1.426 \end{bmatrix}$$

$$i := 0 \, .. \, (N-1)$$
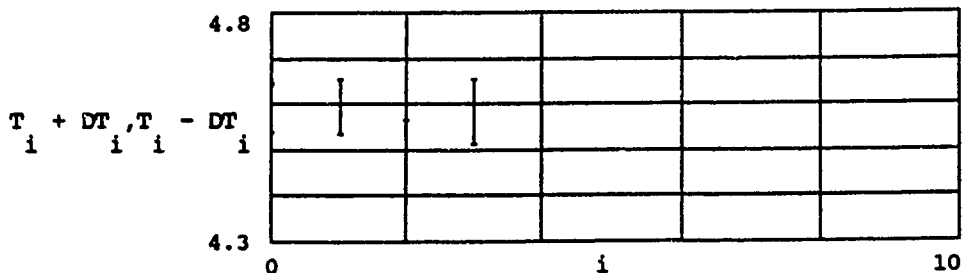
```
@if %1null == null goto nofile
@if not exist %1 goto nofile
copy %1 laser.dat
@del mean.dat
echo %1>tit.tit
echo 1d.e | edlin laser.dat
@copy %1 header.tmp
@echo 2,100de|edlin header.tmp
@print tit.tit
@print header.tmp
mcad laserfit.mcd /m
@echo finished with %1
@del laser.dat
@print title
@print decay.dat
@del tit.tit
@del header.*
@mcad wtmean
@del decay.dat
@goto end
:nofile
@echo Datafile %1 does not exist
:end
```

Appendix II

This appendix gives a detail procedure to obtain the solution of equation (4.1-16) under the condition of (4.1-17) and (4.1-18) in chapter 4. This equation is:

$$i\frac{h}{2\pi}\frac{da_1}{da_2}=-\tilde{V}a_2\exp(i\Omega t)$$

$$i\frac{h}{2\pi}\frac{da_2}{dt}=-\tilde{V}a_1\exp(-i\Omega t) \qquad (1)$$

The initial conditions are:

$$|a_1(0)|^2+|a_2(0)|^2=1$$

$$|a_1(0)|^2=1, \qquad |a_2(0)|^2=0 \qquad (2)$$

We can change the equation (1) into the second order differential equation:

$$\frac{d^2a_1}{d^2t}+i\Omega\frac{da_1}{dt}+(\frac{2\pi\tilde{V}}{h})^2a_1=0 \qquad (3)$$

The solution of above equation can be assumed:

$$a_1=Ae^{-i\alpha t} \qquad (4)$$

Substituting (4) into (3), we get the equation;

70

$$-\alpha^2 + \alpha\Omega + (\frac{2\pi\tilde{V}}{h})^2 = 0 \qquad (5)$$

α can be obtained:

$$\alpha_{1,2} = \frac{\Omega}{2} \pm \frac{1}{2}\sqrt{\Omega^2 + (\frac{4\pi\tilde{V}}{h})^2} \qquad (6)$$

and the general solutions for a_1 and a_2 can be written:

$$a_1 = A\exp(-i\alpha_1 t) + B\exp(-i\alpha_2 t)$$

$$a_2 = -\frac{h}{2\pi\tilde{V}}(\alpha_1 A\exp i(\Omega-\alpha_1)t + \alpha_2 B\exp i(\Omega-\alpha_2)t) \qquad (7)$$

Initial condition: at t=0, a_1=1, a_2=0 and a_1+a_2=1, therefore:

$$A + B = 1$$

$$\alpha_1 A + \alpha_2 B = 0 \qquad (7)$$

The coefficients A and B can be obtained from the equations above:

$$A = \frac{\frac{1}{2}\sqrt{\Omega^2 + (\frac{4\pi\tilde{V}}{h})^2} - \frac{\Omega}{2}}{\sqrt{\Omega^2 + (\frac{4\pi\tilde{V}}{h})^2}}, \qquad B = \frac{\frac{1}{2}\sqrt{\Omega^2 + (\frac{4\pi\tilde{V}}{h})^2} + \frac{\Omega}{2}}{\sqrt{\Omega^2 + (\frac{4\pi\tilde{V}}{h})^2}} \qquad (9)$$

Substituting these coefficients into (7), a_2 can be obtained:

$$a_2 = -\frac{\frac{2\pi \tilde{V}}{h}}{\sqrt{\Omega^2 + (\frac{4\pi \tilde{V}}{h})^2}}[expi(\Omega - \alpha_1)t - expi(\Omega - \alpha_2)t] \qquad (10)$$

and the probability of the system at the upper level is:

$$|a_2|^2 = \frac{2(\frac{2\pi \tilde{V}}{h})}{\Omega^2 + (\frac{4\pi \tilde{V}}{h})^2}(1 - cos(\sqrt{\Omega^2 + (\frac{4\pi \tilde{V}}{h})^2}\ t)) \qquad (11)$$